High-spin state spectroscopy of ^{88,90}Zr

E. K. Warburton, J. W. Olness, C. J. Lister,* and R. W. Zurmühle†
Brookhaven National Laboratory, Upton, New York 11973

J. A. Becker
Lawrence Livermore National Laboratory, Livermore, California 94550
(Received 7 May 1984)

The high-spin states of ^{88}Zr and ^{90}Zr were studied up to ~12-MeV excitation via the ^{74,76}Ge(^{18}O,4nγ)^{88,90}Zr fusion evaporation reactions. Decay schemes were constructed on the basis of gamma-ray excitation functions, angular distribution and linear polarization measurements, γ-γ coincidences, and level lifetimes determined from both Doppler shift attenuation and recoil distance measurements. An effort was made to make as definite spin-parity assignments as possible and to delineate the reliability of these assignments. Probable spins up to ~20$\hbar$ were formed in both nuclei. The experimental results are compared to preliminary results of a large-scale shell model calculation. The yrast spectra of both nuclei can be interpreted as arising from intrinsic modes of excitation with no evidence for collective behavior.

I. INTRODUCTION

States of high angular momentum in nuclei can be formed through intrinsic or collective modes of excitation. The interplay of these methods of generating spin has been the center of considerable interest recently.[1–5] In particular, their relative importance has been found to vary across isotopic chains[6] and also, in some transitional nuclei, has been found to change with excitation energy.

High spin structures in zirconium isotopes with $N \leq 90$ reflect this competition. The lightest isotope so far studied[1] (^{82}Zr) lies in a region where states can be described in terms of collective rotation with a large permanent ground state deformation. ^{84}Zr is more complex, being soft to vibration at low spin, but evolving to a deformed shape at $J \geq 20$.[1] ^{86}Zr appears also to be transitional, but with less collectivity in transitions (^{86}Zr is discussed in the following paper), while ^{88,90}Zr, which are discussed in this paper, appear to be good shell model nuclei, with little or no collective enhancement of transitions and with angular momentum generated solely by the alignment of individual nucleons.

This paper reports part of our systematic survey of yrast and near yrast states in Zr isotopes which has been made to map out the transition from purely intrinsic to highly collective modes of excitation. Results for ^{84}Zr have already been published while data collected on ^{82,83,86}Zr are under analysis.[1] These data, together with recent studies of Kr (Ref. 7), Rb (Ref. 8), and Sr (Ref. 1) isotopes, now form a considerable body of data on high spin states in this region.

^{88}Nb (Ref. 9) and ^{90}Nb (Ref. 10) both have $J^{\pi}=8^{+}$ ground states which decay to ^{88}Zr and ^{90}Zr by β^{+}/EC decay. Because of the high ^{88,90}Nb ground state spins the low-lying high-spin ($J \leq 9$) spectra of both Zr nuclei can be investigated by β^{+}/EC decay; such studies have been made up to ~5.8-MeV excitation in ^{88}Zr and 5.6-MeV excitation in ^{90}Zr, respectively.[11,12] ^{90}Nb(β^{+}/EC)^{90}Zr, most recently studied by Warburton and Alburger,[11] provides all that is known about the high-spin levels of ^{90}Zr. This is rather surprising since ^{90}Zr lies in the valley of stability and is relatively easy to produce as well as being of special interest because it is doubly magic. Spectroscopy of high spin states in ^{88}Zr has been previously investigated by Kitching *et al.*[13] using the ^{86}Sr(α,2n)^{88}Zr and ^{89}Y(p,2n)^{88}Zr reactions and by Numao *et al.*[14] using the ^{86}Sr(α,2n)^{88}Zr reaction. These studies provided information on ^{88}Zr levels up to ~6-MeV excitation and $J \leq 14$. The present study has been done with the ^{74,76}Ge(^{18}O,4n)^{88,90}Zr reactions and, as was certainly to be expected, consideration of the kinematics leaves no doubt that states with considerably higher excitation energies and spin values can be formed with the (^{18}O,4n) reaction than in the previous studies.

The determination of spin-parity assignments via fusion-evaporation reactions is based in large part on the mechanism for this type of reaction: this mechanism is well known and the assignments are unusually reliable. However, it is often hard for an interested reader to apprise the reliability of a particular assignment. A particular effort was made in this report to describe the basis for spin-parity assignments and to delineate their reliability.

II. EXPERIMENTAL PROCEDURE AND ANALYSIS

Experimental measurements were performed of (1) γ-ray yield at 90° for seven ^{18}O bombarding energies between 40 and 80 MeV; (2) γ-γ coincidences; (3) γ-ray angular distributions; (4) γ-ray linear polarizations; (5) level lifetimes via the DSAM (Doppler-shift attenuation method); and (6) level lifetimes via the RDM (recoil-distance method). Targets for (1)—(5) were prepared by the reduction of enriched or natural GeO in a quartz boat and in a hydrogen atmosphere followed by vacuum evaporation of the resulting Ge metal to a thickness of ~1 mg/cm^2 onto 35-mg/cm^2 Pb backings. Some measurements were also made using a target of 0.8-mm thick

natural Ge (20.7% ^{70}Ge, 27.5% ^{72}Ge, 7.3% ^{73}Ge, 36.4% ^{74}Ge, and 7.7% ^{76}Ge). Experiments utilized one, two, or three coaxial intrinsic Ge or Ge(Li) detectors of 12—19 % efficiency [relative to a 7.62×7.62-cm NaI(Tl) detector] and resolution of 1.9—2.1 keV FWHM (full width at half maximum) for the 1.33-MeV ^{60}Co γ ray. Two small planar detectors were used for detection of low-energy γ rays: (1) an intrinsic Ge low-energy photon spectrometer (LEPS) with a resolution of 600 eV (FWHM) at 122 keV, and (2) a silicon detector with a resolution of 210 eV (FWHM) at 6.4 keV. The major part of the reduction of γ-ray spectra to γ-ray peak positions and intensities was done using the least-squares fitting program SAMPO.[15] For each measurement the detector efficiencies were determined *in situ* with standard radioactive γ-ray intensity standards such as ^{152}Eu and ^{56}Co. Gamma-ray energies were determined by the mixed-source technique relative to adopted γ-ray energy standards[16] and precision energies of ^{90}Zr γ transitions.[12] ^{18}O beams were produced by the Brookhaven National Laboratory (BNL) Tandem Van de Graaff facility. Data collection and analyses were done using the BNL Sigma VII computer facility.[17]

A. Excitation functions and relative yields

For these measurements a coaxial detector and the LEPS were placed at 90° to the beam on opposite sides of the target and ~12 cm from it. The enriched ^{74}Ge and ^{76}Ge targets were backed with 9 mm of Cu and were oriented at 45° to the beam with the Ge side facing the LEPS. Spectra were recorded for each target at $E(^{18}\text{O})=40$, 45, 50, 55, 60, 70, and 80 MeV. The integrated beam charge accumulated at each energy determined the relative normalization.

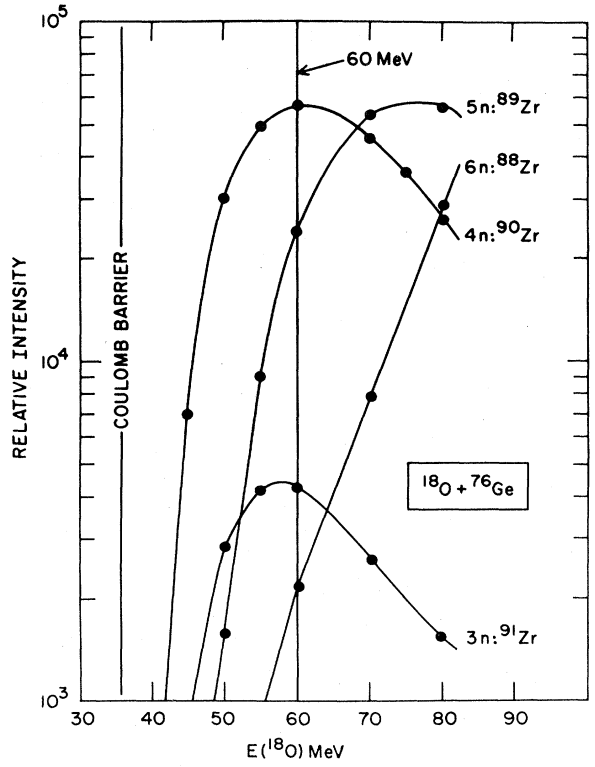

FIG. 1. Relative yield as a function of bombarding energy for the production of Zr isotopes by ^{18}O bombardment of ^{76}Ge. The number of outgoing neutrons and the final Zr isotope are identified as is the Coulomb barrier for $^{18}\text{O}+^{76}\text{Ge}$. The curve through the data points is solely to guide the eye. Most of the present measurements were made at $E(^{18}\text{O})=60$ MeV.

The γ-ray excitation functions are *qualitatively* consistent with expectations from previous results (see, e.g., Ref. 18) and predictions of the statistical model computer code CASCADE.[19] The results are exemplified in Fig. 1 which displays the relative $^{76}\text{Ge}(^{18}\text{O},x\text{n}\gamma)$ yield into the ground state of the final Zr isotope for $x=3$, 4, 5, and 6. For any of these xn channels, the yield for the Y isotope formed by substitution of a proton for a neutron has an excitation function essentially undistinguishable in shape, while an α particle in the evaporation channel effectively acts as ~1.5 nucleons, e.g., the yield for the 3nα channel peaks at an energy about halfway between the energy of the peak yields for the 4n and 5n channels.

The results for $^{18}\text{O}+^{74}\text{Ge}$ are similar in shape to those for $^{18}\text{O}+^{76}\text{Ge}$ but displaced somewhat in $E(^{18}\text{O})$. If $E_{\max}$ is the value of $E(^{18}\text{O})$ at which the yield for a particular γ transition is at a maximum, then we find that the yield curve results for $^{74,76}(^{18}\text{O},4\text{n})^{88,90}$Zr can be parametrized by

$$^{88}\text{Zr}: \; E_{\max}(\text{MeV})=(60\pm2)+(2.0\pm0.3)E_x(\text{MeV}) ,$$
$$^{90}\text{Zr}: \; E_{\max}(\text{MeV})=(54\pm1)+(1.65\pm0.33)E_x(\text{MeV}) , \quad (1)$$

where E_x is the excitation energy of the level emitting the transition. The difference of ~6 MeV in the values of $E_{\max}$ for the ground states can be explained by the differ-

TABLE I. Relative production cross sections in $^{74,76}\text{Ge}(^{18}\text{O},x\text{n}y\text{p}z\alpha)$ for $E(^{18}\text{O})=60$ MeV.

Outgoing channel	Residual nucleus and relative cross section[a]			
	$^{74}\text{Ge}+^{18}\text{O}$		$^{76}\text{Ge}+^{18}\text{O}$	
nα	^{87}Sr	<2	^{89}Sr	11
2nα	^{86}Sr	83	^{88}Sr	18
3nα	^{85}Sr	133	^{87}Sr	128
4nα	^{84}Sr	8	^{86}Sr	49
2np	^{89}Y	25	^{91}Y	5
3np	^{88}Y	392	^{90}Y	97
4np	^{87}Y	89	^{89}Y	50
5np	^{86}Y	5	^{88}Y	35
2n	^{90}Zr	6	^{92}Zr	18
3n	^{89}Zr	155	^{91}Zr	67
4n	^{88}Zr	1000	^{90}Zr	1000
5n	^{87}Zr	38	^{89}Zr	412
6n	^{86}Zr	6	^{88}Zr	66

[a]The isotopic composition of the nominal ^{74,76}Ge targets was (A,%): ^{74}Ge (70, 0.26; 72, 0.69; 74, 98.90; 76, 0.15), ^{76}Ge (70, 1.30; 72, 2.00; 73, 0.63; 74, 3.25; 76, 92.82).

ence in the thresholds for the two reactions which are 28.29 and 21.79 MeV for ^{74,76}Ge(^{18}O,4n)^{88,90}Zr, respectively.

The relative yield of different outgoing channels is summarized in Table I for $E(^{18}O)=60$ MeV, the bombardment energy at which most of the measurements reported herein were made. The relative yields have been corrected for the γ-ray angular distributions and relative detector efficiencies. We assume negligible direct feeding of the ground states. The results have not been corrected for the contributions from other Ge isotopes in the predominantly ^{74}Ge and ^{76}Ge targets. (An estimate of this effect is included in the results of Fig. 1.)

B. Gamma-gamma coincidence measurements

Gamma-gamma coincidence measurements were performed at $E(^{18}O)=60$ MeV with the ^{74}Ge, ^{76}Ge, and natural Ge targets mounted relative to the beam as described in the last subsection (Sec. II A). For the major measurements one coaxial Ge detector was placed at 0° to the beam, and two were positioned at 90° and on opposite sides of the target. Conical lead shields reduced the scattering of γ rays between detectors. The counting rate in each detector was approximately 5 kHz. Time-to-amplitude converter (TAC) spectra were formed for one 90° detector ($G1$) in coincidence with either the other 90° detector ($G2$) or the 0° detector ($G3$). Singles spectra ($4K$) for $G1$ and $G3$ and total coincidence spectra ($4K$) for $G1$-$G2$ and $G1$-$G3$ are actively recorded (i.e., on line) as well as the two TAC spectra ($1K$). The TAC-E_{G1}-E_{G2} and TAC-E_{G1}-E_{G3} matrices were accumulated event by event on magnetic tape (EMR). Twenty-four hours of data were accumulated for both the ^{74}Ge and ^{76}Ge targets. The measurement with the natural Ge target lasted about four hours and was performed with $G1$ replaced by the

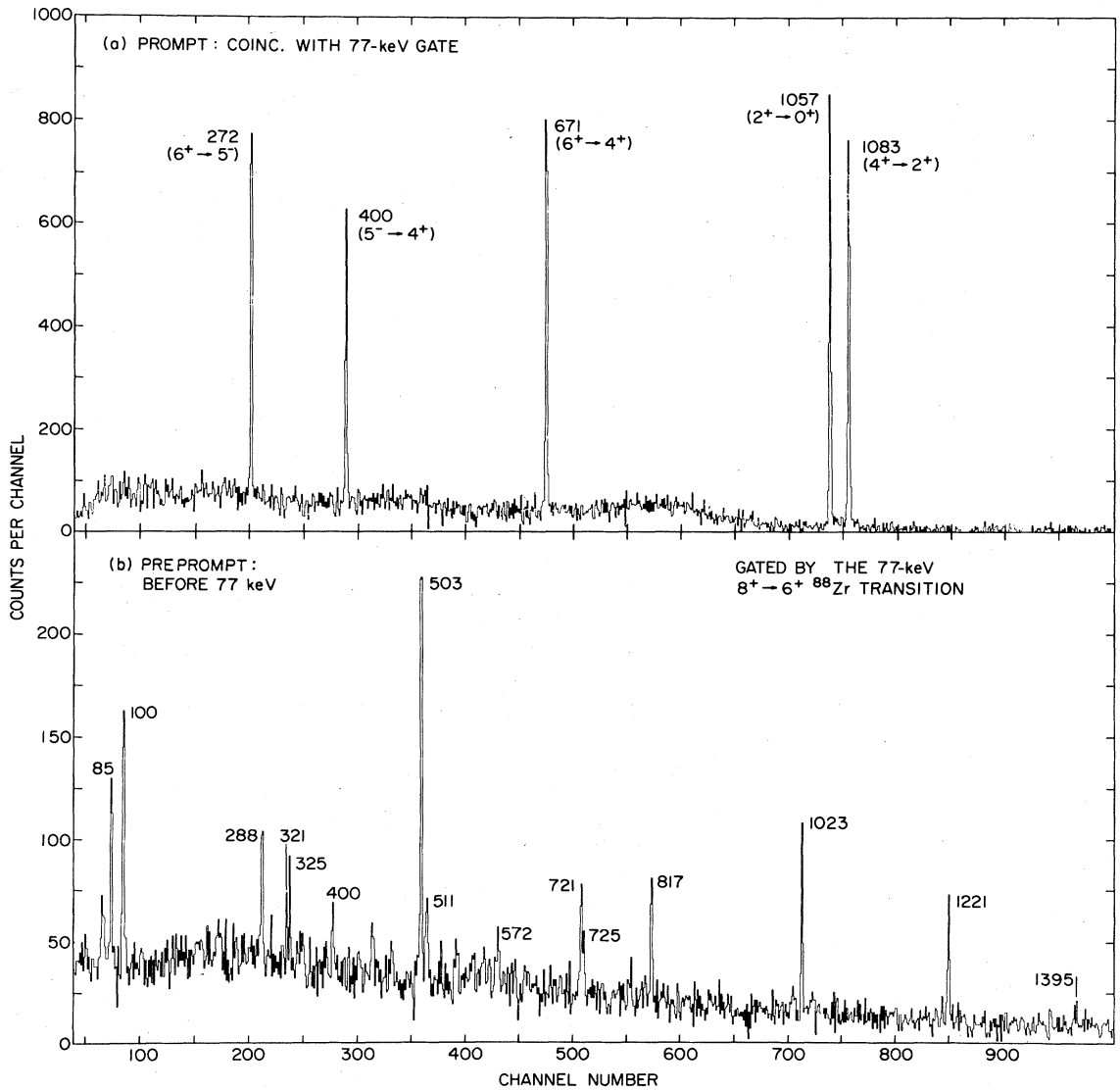

FIG. 2. Portions of 2048-channel spectra in coincidence with the 77-keV $8^+ \rightarrow 6^+$ decay of the 1.7-s isomeric 2887-keV level of ^{88}Zr. Prompt coincidences are shown in (a), while (b) displays γ rays emitted preceding the 77-keV transition by 0.32-0.70 μs. ^{88}Zr transitions are identified by their energies in keV.

LEPS. The purpose of this latter measurement was to obtain more precise data on the placement of γ rays with $E_\gamma < 300$ keV.

The time dispersion of the TAC spectrum was ~ 1 ns/channel while the γ-γ time resolution was ~ 15 ns FWHM. Since 1024-channel TAC spectra were recorded, it was possible in subsequent analysis of the EMR data to search for γ rays preceding or following any given γ ray by ~ 0.5 μs as well as those in prompt coincidence. An example is shown in Fig. 2 which displays the energy spectrum ($G2$) gated by an energy window (background subtracted) set on the ^{88}Zr 77-keV $8_1^+ \rightarrow 6_1^+$ transition in

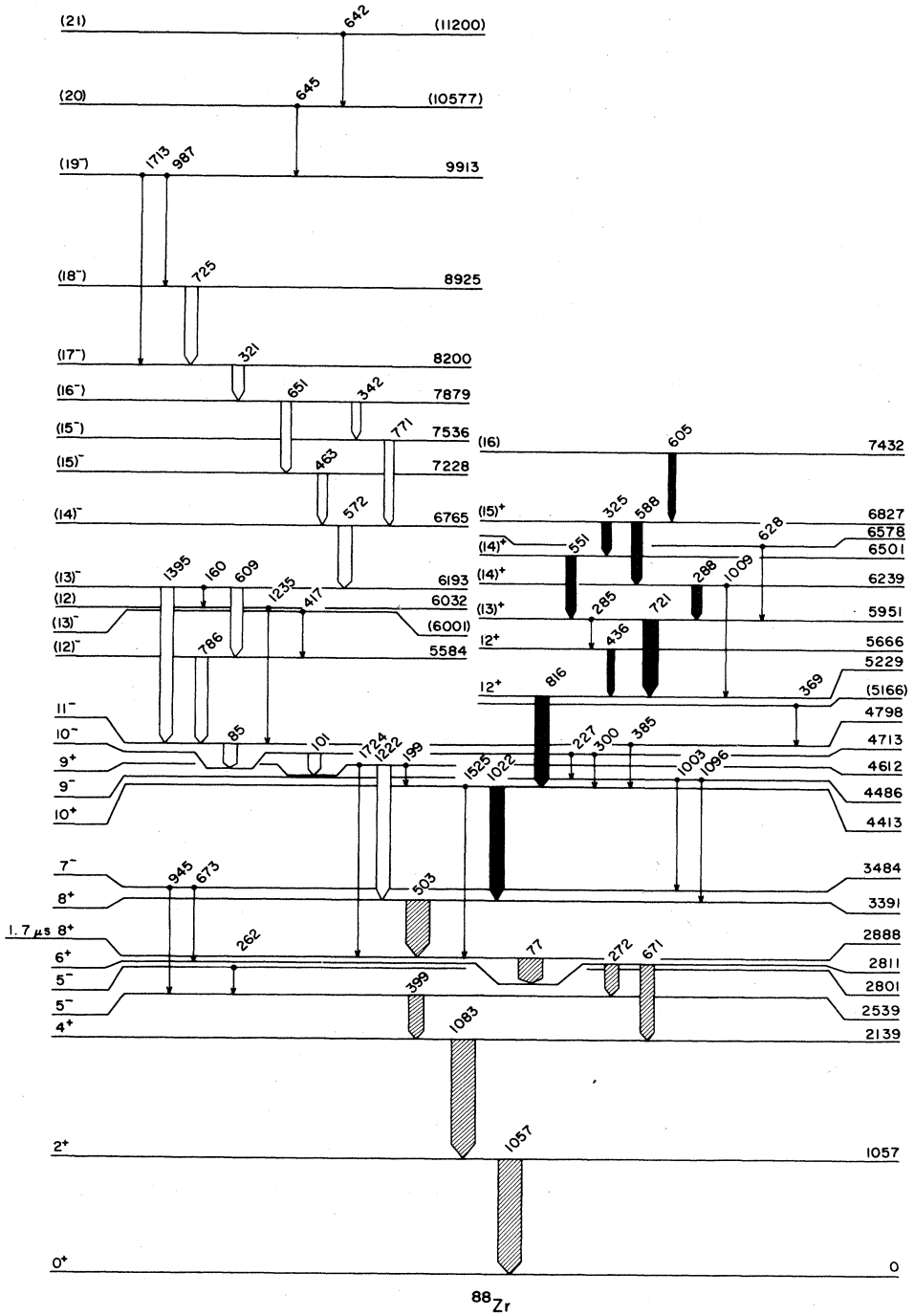

FIG. 3. Level scheme for ^{88}Zr showing excitation energies and γ-transition energies (in keV) for levels populated in the ^{74}Ge(^{18}O,4n)^{88}Zr reaction only. The γ intensities are roughly proportional to the width of the arrows. Above the 3391-keV level there appear to be two groupings of levels; even parity to the left and odd parity to the right. Qualifications on the placement of transitions and the existence of levels are given in the footnotes to Table II. A further qualification is necessary for the levels between 6193 and 9913 keV on the left. Although six levels are definitely populated in this region, there are several possible orderings of the γ transitions and thus of the level positions. The one shown is only marginally the most probable.

the LEPS ($G1$) spectrum. In this case, energy spectra were formed in coincidence with the TAC in both prompt (-64 to $+64$ ns) and preprompt (-0.32 to -0.70 μs) time bins.

Although all the measurements reported herein contributed to the final decay schemes proposed for ^{88}Zr (Fig. 3) and ^{90}Zr (Fig. 4), the γ-γ coincidence measurement was overwhelmingly the most important. For both ^{88}Zr and ^{90}Zr, the lowest-lying 8^+ state is isomeric (see Figs. 3 and 4) and a problem in establishing the high-spin decay scheme is the inherently low sensitivity for identifying decays into this state. Another method was attempted in addition to searching for prepromt transitions in coincidence with γ decays of the 8^+ isomer (e.g., Fig. 2). A thin Ge target-backing combination was used and the Zr recoils were caught on a Ta foil 15 cm ($\sim$30 ns) downstream from the target. Coincidences were then formed between a Ge detector viewing only the target and another viewing only the catcher foil. This procedure eliminated prompt-prompt γ-γ coincidences. The sensitivity of this method was limited by the Doppler broadening of the prompt γ rays and it was found for the range of lifetimes

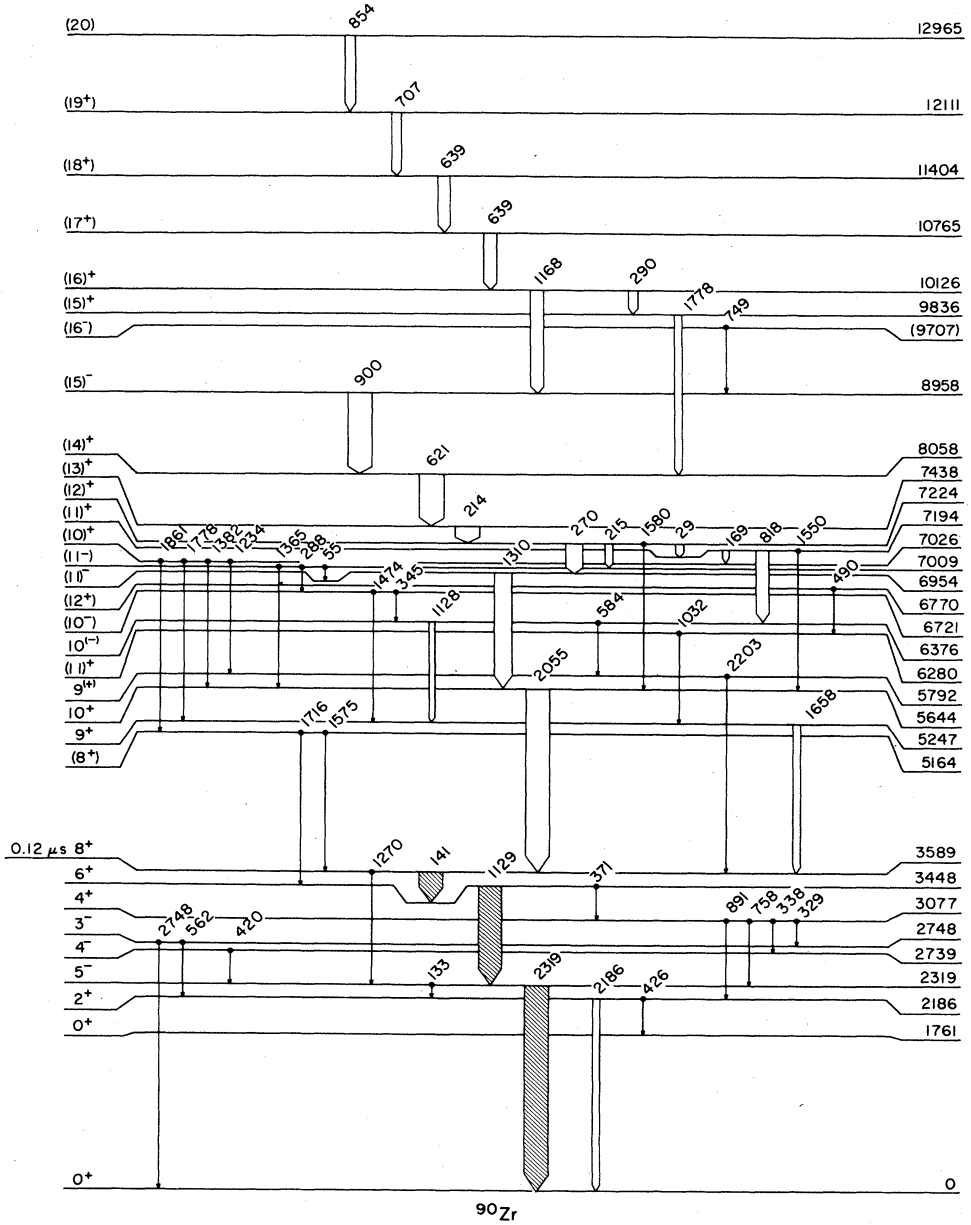

FIG. 4. Level scheme for ^{90}Zr showing excitation energies and γ-transition energies (in keV) for levels populated in the ^{76}Ge(^{18}O,4n)^{90}Zr reaction only. The γ intensities are roughly proportional to the width of the arrows. Qualifications on the placement of transitions and the existence of levels are given in the footnotes to Table III.

encountered in ^{88,90}Zr that the prompt-preprompt timing method with a backed target gave the best sensitivity for detecting γ transitions into the 8^+ isomer.

C. Gamma-ray angular distributions and attenuated Doppler-shift measurements

Angular distributions were obtained simultaneously with a coaxial Ge detector and the LEPS detector for both ^{74}Ge and ^{76}Ge targets. The LEPS was 15.7 cm from the target (which had its normal 45° to the beam) and viewed the front of the target at angles to the beam (θ_γ) of 90°, 110°, 120°, 127.5°, and 135°. The Ge detector was 10 cm from the target and viewed it through its backing at θ_γ=0°, 30°, 45°, 60°, and 90°. The relative normalization of the various spectra was determined to first order using the integrated beam charge. However, several convenient long-lived isomers were found for which the intensity of subsequent γ decay provided a more accurate normalization since their use corrected for effects due to misalignments, changes in the beam direction and intensity, target inhomogeneities, etc. The principal isomers used were the 13.9-ms 8^+ 675-keV state of ^{88}Y (Ref. 9), which decays by a cascade of 443-232 keV; the 16.1-s $\frac{9}{2}^+$ 909-keV state of ^{89}Y (Ref. 20), which decays to the ground state; and the 0.81-s 5^- 2319-keV state of ^{90}Zr (Ref. 10), which also ground-state decays. Several other long-lived states also provided checks on the normalization.

The reduced angular distribution data were fit to the Legendre polynomial expansion

$$W(\theta_\gamma)=I_\gamma[1+A_2P_2(\cos\theta_\gamma)+A_4P_4(\cos\theta_\gamma)] . \quad (2)$$

Representative data are shown in Fig. 5. The angular distributions also yielded DSAM information, since the average γ-ray energy can be determined as a function of angle to obtain information on the attenuation factor

$$F(\tau)=[\langle E_\gamma(t)\rangle-E_{\gamma 0}]/[E_\gamma(0)-E_{\gamma 0}] , \quad (3)$$

where the average γ-ray energy is determined by the time integral of the γ-ray energy

$$E_\gamma(t)=E_{\gamma 0}[1+\beta(t)\cos\theta_\gamma] \quad (4)$$

over the slowing down of the recoiling ions from velocity $\beta(0)$ to velocity $\beta(\infty)\equiv 0$, where $\beta(t)=v(t)/c$ and $E_{\gamma 0}\equiv E_\gamma(\infty)$. The values of $[E_\gamma(0)-E_{\gamma 0}]$ used in Eq. (3) were evaluated from the RDM data described in Sec. II E. Specifically, at each angle of the angular distribution measurements the centroid energy $\langle E_\gamma(\theta_\gamma)\rangle$ of the Doppler shifted line shape was extracted and the experimental values of $\langle E_\gamma(\theta_\gamma)\rangle$ were then fitted as a function of $\cos\theta_\gamma$ to determine the best value of $F(\tau)$ via Eqs. (3) and (4).

Tables II and III contain a condensation of all the experimental results obtained for ^{88,90}Zr. The decay schemes of Figs. 3 and 4 and the more detailed information summarized in Tables II and III are based mainly on analyses of the γ-γ coincidence and angular distribution data. Referring to the tables, the E_γ ($\equiv E_{\gamma 0}$) were derived using Eq. (4) and the $F(\tau)$ were evaluated using Eq. (3). Arguments for the spin-parity assignments are described in Sec. III. The I_f are the net side feedings, i.e., the net ΣI_γ(out)$-\Sigma I_\gamma$(in) for each level. The I_f and the level excitation energies were calculated by a least-squares fit to all the γ-ray energies and intensities.

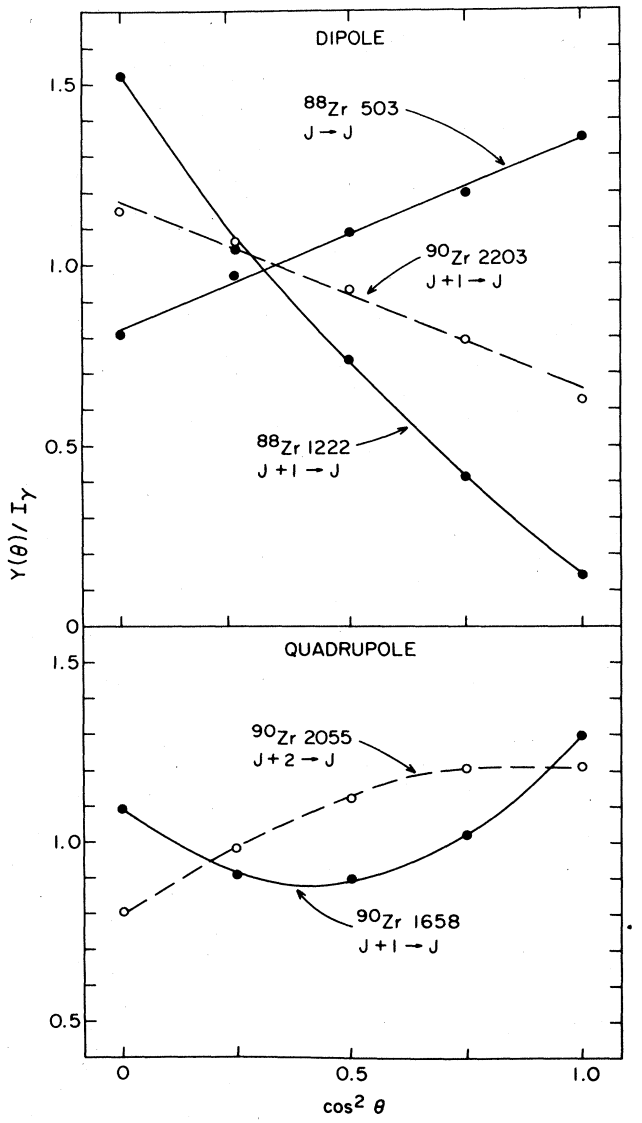

FIG. 5. Representative γ-ray angular distributions observed in the ^{74,76}Ge(^{18}O,4n)^{88,90}Zr reactions. The ^{88}Zr 503-keV and ^{90}Zr 2203-keV transitions have typical (pure dipole) $J\rightarrow J$ and $J+1\rightarrow J$ patterns, while the ^{90}Zr 2055-keV transition has the classic shape of a $J+2\rightarrow J$ quadrupole transition. The ^{88}Zr 1222-keV and ^{90}Zr 1658-keV angular distributions are examples of mixed quadrupole-dipole transitions. The error bars are smaller than the data points.

D. Gamma-ray linear polarization

Gamma-ray linear polarization measurements were performed with a Compton scattering polarimeter[21] consisting of two horizontally mounted coaxial Ge detectors placed on a turntable beneath the beam line. The detec-

TABLE II. ^{88}Zr energy levels, lifetimes, and γ-ray transitions deduced from ^{74}Ge(^{18}O,4n)^{88}Zr.

					Angular distribution[d,e]						
J_i^{π}[a]	E_i[b] (keV)	E_f (keV)	E_γ[c] (keV)	I_γ	A_2 (%)	A_4 (%)	I_f[f] ($\times 10^{-2}$)	$P(\%)$[g,e] expt	th	$F(\tau)$[h] (%)	τ (ps)
2^+	1056.972(50)	0	1056.965(50)	28390±700	+14.5(11)	−2.8(12)	10(10)	+22(2)	+22(2);$E2$	0	
4^+	2139.489(60)	1057	1082.510(50)	27410±685	+15(1)	−3.5(11)	11(9)	+23(2)	+22(2);$E2$	0	
5^-	2538.900(70)	2139	399.410(35)[i]	(9815±500)	−11(2)	0(4)	0(4)	+17(3)	+16(3);$E1$	0	
5^-	2800.63(12)	2539	261.73(10)	520±50	+10(7)	0	5(5)	+42(36)	+16(12);$M1$	0	
6^+	2810.705(70)	2539	271.805(20)	8680±350	−13(3)	0	0(13)	+14(4)	+18(3);$E1$	0	
		2139	671.215(50)[j]	16500±500	+13.7(12)	−2.4(12)		+20(3)	+21(2);$E2$	0	
8^+	2887.70(7)	2811	76.993(10)	25100±740[k]	+14(2)	0	51(12)		;$E2$	0	
8^+	3390.61(8)	2888	502.917(40)	19960±500	+34(2)	0(2)	14(7)	+56(7)	+61(5);$M1$	RDM	30(2)
7^-	3483.53(13)	2811	(672.82)[l]	(500±200)[l]			5(2)		;$E1$		
		2539	(944.62)[m]	(675±70)	+4(4)	0		+41(9)	+7(7);$E2$	0	
10^+	4413.03(11)	3391	(1022.42)[n]	(12200±350)	+31(3)	−9(3)	14(5)	+47(4)	+57(5);$E2$	RDM	<2
		2888	[1525.14(20)]	220±30	+37(8)	0			;$E2$	0	
9^-	4486.20(11)	3484	1002.667(70)	720±30	+35(4)	−4(4)	0(2)	+10(30)	+63(12);$E2$	0	
		3391	1095.585(70)	480±20	−29(3)	0		+19(44)	+39(12);$E1$	0	
9^+	4612.24(9)	4413	[199.19(10)]	110±30	−60(30)	0	4(3)	−19(19)	−68(50;$M1$		<250
		3391	1221.630(50)	5870±180	−94(3)	+9(4)		+15(5)	−91(3);$M1$	RDM	
		2888	[1724.49(20)]	240±50	−17(6)	0		−37(30)	−23(22);$M1$	0	
10^-	4713.02(10)	4612	100.787(20)	5870±180[o]	−27(5)	0	10(6)	+31(3)	+33(6);$E1$	RDM	3250(250)
		4486	(226.82)[p]	(1208±150)[p]	−36(4)	0		−13(6)	−45(6);$M1$	0	
		4413	299.92(15)	490±50	+39(8)	0		−34(17)	−73(18);$E1$	0	
11^-	4797.57(10)	4713	84.550(25)[q]	6500±500	−25(6)	0	14(6)	−29(4)	−33(7);$M1$	RDM	72(6)
		4413	384.538(90)	880±45	−32(4)	0		+35(4)	+41(6);$E1$	0	
[12]	(5166.1(5))	4798	368.55(40)[r]	(400±200)	−9(4)	0	4(2)	−18(5)	−13(10);$M1$	30(2)	0.95(20)
12^+	5229.44(13)	4798	(431.86)	<250			5(4)				15(1)
		4713	(516.41)	<90							
		4413	816.398(70)	9915±250	+32(3)	−12(3)		+51(4)	+51(6);$E2$	RDM	
$(12)^-$	5583.80(12)	5229	(354.36)	<50			7(2)				<1.0
		4798	786.131(70)	3000±100	−22(4)	0		−9(13)	−30(6);$M1$	32(2)	
		4413	(1170.76)	<44							
12^+	5665.89(15)	5229	436.490(70)[s]	(1890±110)[s]	−2(5)	−1(6)	16(2)	+27(11)	+4(18);$M1$	51(3)	0.40(15)
$(13)^+$	5950.75(16)	5666	285.19(20)	270±30	−33(6)	0	7(4)	−18(13)	−68(14);$M1$		<0.15
		5229	721.23(15)	7100±240	−33(2)	+1(2)		−21(4)	−43(10);$M1$	42(3)	
$(13)^-$	(6000.8(4))	5584	416.97(30)[t]	(930±80)[t]	−33(6)	0	9(1)	−19(16)	−42(7);$M1$	30(3)	<1.0
(12)	(6032.47(12))[u]	4798	1234.92(15)	315±30	−68(24)	0	0(1)			0	
$(13)^-$	6192.88(11)	6033	160.418(30)[v]	315±30[v]	−37(4)	0	3(2)			0	2.45(20)
		5584	608.90(10)[w]	(1090±60)[w]	−33(10)	0		−34(24)	−32(12);$M1$	RDM	
		4798	1395.385(70)	2000±100	+27(2)	−9(2)		+62(9)	+43(7);$E2$	RDM	
$(14)^+$	6238.79(16)	5951	288.048(40)	3500±100	−28(2)	0	6(2)	−27(2)	−37(4);$M1$	15(4)	1.5(4)
		5229	1009.25(15)	755±40	>0	0				15(15)	

TABLE II. (*Continued*).

J_i^{π}[a]	E_i[b] (keV)	E_f (keV)	E_γ[c] (keV)	Angular distribution[d,e] I_γ	A_2 (%)	A_4 (%)	I_f[f] ($\times 10^{-2}$)	$P(\%)$[g,e] expt	th	$F(\tau)$[h] (%)	τ (ps)
$(14)^+$	6501.32(24)	5951	550.58(30)	2630±130	−27(4)	0	15(2)	−46(6)	−36(4);$M1$	63(2)	0.23(5)
[14]	6578.3(6)	5951	627.5(5)[x]	(500±200)[x]			5(2)	+18(5)			
$(14)^-$	6765.18(23)	6193	572.39(20)[y]	3140±100	−43(3)	+2(3)	0(2)	−13(8)	−53(4);$M1$	42(2)	≤0.70
$(15)^+$	6826.65(24)	6501	325.34(10)	1180±50	−25(2)	0	32(3)	−28(6)	−33(3);$M1$	73(4)	0.15(3)
		6239	587.85(20)	3530±200	+0(30)	0		−15(16)	+0(42);$M1$	90(20)	
$(15)^-$	7228.0(3)	6765	462.87(20)	1900±150	−23(2)	+2(3)	10(3)	−23(6)	−31(3);$M1$	32(3)	≤1.1
(16)	7431.8(4)	6827	605.15(30)[z]	(1540±200)[z]	−22(12)	0	15(2)		−30(14);$M1$	79(2)	0.15(4)
(15^-)	7536.4(4)	6765	771.12(30)	1300±150	−21(8)	0	3(3)	−15(27)	−29(9);$M1$	53(2)	≤0.48
		6239	(1297.6)	<120							
(16^-)	7878.8(4)	7536	342.23(40)[aa]	(1070±200)[aa]	−36(10)	0	1(3)	−27(8)	−46(12);$M1$	42(3)	≤0.70
		7228	650.93(40)	920±200	−50(20)	0		−23(16)	−60(20);$M1$	>15	
(17^-)	8200.1(5)	7879	321.30(20)	1870±80	−22(2)	+2(2)	1(6)	−31(4)	−25(3);$M1$	42(6)	0.4(6/2)
(18^-)	8925.0(5)	8200	724.85(20)[bb]	(1800±600)[bb]	−33(10)	0	12(6)	−20(7)	−42(11);$M1$	>30	<0.5
(19^-)	9912.5(5)[cc]	8925	987.35(20)	550±100	−34(12)	0	3(4)	−4(20)	−44(18);$M1$	<20	>1.0
		8200	1712.50(20)	590±40	+22(6)	−8(6)		+41(26)	+33(18);$E2$	<20	
(20)	(10557.2(9))[dd]	9912	644.7(7)[ee]	(840±300)[ee]			3(4)	−11(12)		≥50	≤0.2
(21)	(11199.6(11))[dd]	10557	642.4(7)[ff]	(550±200)[ff]	−40(25)	0	6(2)	−12(12)	−50(30);$M1$	60(25)	0.32(20)

[a]See the text.

[b]Corrected for recoil. The uncertainty in the least significant figure is given in parentheses. E_i completely enclosed in parentheses are to some degree speculative.

[c]Not corrected for recoil. Energies enclosed in parentheses are calculated from $E_i - E_f$. Those in square brackets were not positively identified in the $\gamma\gamma$ coincidence data and thus are somewhat uncertain.

[d]The relative intensity I_γ is corrected for the relative γ-ray efficiency and is in arbitrary units. Intensities given in parentheses were extracted from unresolved multiplets using auxiliary information (excitation functions, coincidence data, etc.). Intensities in square brackets were estimated. An entry of 0 for A_4 means the fit was to $I_\gamma(1+A_2P_2)$ only, i.e., χ^2 was not significantly improved by the inclusion of an A_4 term.

[e]In the case of unresolved doublets an attempt has been made to correct A_2, A_4, P, and $F(\tau)$ for the other member of the doublet unless otherwise footnoted. These corrections made use of all the ^{74,76}Ge + ^{18}O angular distribution, linear polarization, and excitation function data.

[f]Relative side feeding of the level in question in units of $100I_\gamma$.

[g]The linear polarization (see the text). The theoretical (th) value is calculated assuming the indicated pure multipole.

[h]The Doppler shift attenuation factor. [An entry RDM means $F(\tau)=0$ and τ was measured by the recoil distance method.]

[i]Doublet with the ^{87}Y 2827→2428 transition. I_γ(total)=11420±260.

[j]Doublet with the essentially negligible ^{88}Zr 3484→2811 transition.

[k]Calculated from an observed intensity of 6450±190 using a total conversion coefficient of 2.892 (see the text).

[l]See footnote j.

[m]Doublet with the ^{88}Y 3257→2312 transition. I_γ(total)=1130±60. A_2 and P are for the composite peak.

[n]Triplet with the 2428→1404→381 1023-keV doublet in ^{87}Y. I_γ(total)=14400±350.

[o]The total intensity was calculated using $\alpha(E1)=0.1112$.

TABLE II. (*Continued*).

[p]Doublet with a ^{86}Sr transition. I_γ(total)=1930±100. A_2 and P are for the composite peak.
[q]Doublet with the Pb x ray. E_γ and I_γ were determined relative to the ^{88}Zr 100-keV γ ray from spectra taken with a thick natural Ge target. The total transition intensity was calculated with $\alpha(M1)=0.3253$.
[r]Doublet with the ^{85}Sr 3397→3028 transition. I_γ(total)=1450±70. A_2, P, and $F(\tau)$ are for the composite peak.
[s]Doublet with an unassigned ^{88}Y transition. I_γ(total)=2430±100. A_2, P, and $F(\tau)$ are for the composite peak.
[t]Doublet with the ^{87}Sr 3249→2831 transition. I_γ(total)=1100±70.
[u]It is almost as likely that the order of the 1235- and 160-keV transitions is reversed in which case the 6032-keV level would be at 4950.0 keV.
[v]The total transition intensity was calculated using $\alpha(M1)=0.0292$.
[w]Doublet with the 608.40(5)-keV 1204→596 transition in ^{74}Ge. I_γ(total)=1540±50.
[x]Triplet with the ^{85}Sr 3028→2401 and ^{86}Sr 2858→2231 transitions. I_γ(total)=3570±160. P is for the composite peak.
[y]Any other branch is less than 10% of this one.
[z]Doublet with an unassigned ^{87}Y transition. I_γ(total)=1760±180. A_2 is for the composite peak.
[aa]Doublet with the ^{89}Y 4793→4450 transition. I_γ(total)=1790±180.
[bb]Doublet with the ^{87}Y 3553→2827 transition. I_γ(total)=2220±100.
[cc]This level is quite certain. However, because of uncertainty in the ordering of cascades, the placement of the levels between 7 and 9.6 MeV is uncertain.
[dd]The association of such a transition with ^{88}Zr is certain; the placement in the level scheme is highly speculative.
[ee]Triplet with the ^{88}Y 4824→4178 transition and the ^{90}Zr doublet (see Table III). I_γ and $F(\tau)$ are from $\gamma\gamma$ only. I_γ(total)=5000±200. P is for the composite peak.
[ff]Doublet with the ^{89}Zr 5378→4736 transition. I_γ(total)=700±150.

TABLE III. ^{90}Zr energy levels and γ-ray transitions deduced from ^{76}Ge(^{18}O,4n)^{90}Zr.

				Angular distribution[d,e]						
J_i^{π}[a]	E_i[b] (keV)	E_f (keV)	E_γ[c,i] (keV)	I_γ	A_2 (%)	A_4 (%)	I_f[f] ($\times10^{-2}$)	$P(\%)$[g,e] expt	th	$F(\tau)$[h] (%)	τ (ps)
2^+	2186.282(10)	1761	(425.59(20))	[14]			0(5)	0(9)	+2(3);$E2$	0.00	
		0	2186.254(10)	6960±200	+2(2)	−3(2)				0.00	
5^-	2319.000(10)	2186	132.718(3)	1650±100[j]	+1(1)	+1(1)	25(14)			0.00	
		0	2318.968(10)	30600±760	0[k]	0[k]		−1(3)	0	0.00	
4^-	2739.289(50)	2319	(420.288(50))	[12]			0				
3^-	2747.834(24)	2186	(561.549(23))	[55]			0				
		0	(2747.792(25))	[3]							
4^+	3076.894(13)	2748	(329.060(23))	[58]			3(1)				
		2739	(337.606(50))	[12]							
		2319	(757.891(8))	[18]							
		2186	890.607(8)	830±50	+15(4)	−2(4)				0.00	
6^+	3448.187(13)	3077	371.292(7)	610±50	+27(5)	+4(5)	0(17)			0.00	
		2319	1129.180(7)	(34000±1125)[l]	−20(1)	+1(2)		+22(3)	+27(2);$E1$	0.00	
8^+	3589.439(13)	3448	141.252(2)	(26000±960)[m]	+23(3)	−7(3)	100(15)	+32(3)	+32(6);$E2$	0.00	
		2319	1270.430(7)	520±40	+44(15)	0				0.00	

TABLE III. (*Continued*).

J_i^{π}[a]	E_i[b] (keV)	E_f (keV)	E_γ[c,i] (keV)	Angular distribution[d,e] I_γ	A_2 (%)	A_4 (%)	I_f[f] ($\times 10^{-2}$)	$P(\%)$[g,e] expt	th	$F(\tau)$[h] (%)	τ (ps)
(8^+)	5164.458(19)	3589	1575.004(15)	300±50			2(1)			0.00	
		3448	1716.253(15)	400±70						0.00	
9^+	5247.491(24)	3589	1658.035(20)[n]	(9500±500)[n]	+4(4)	+30(5)	0(9)	+7(5)[m]	+6(6);$M1$	RDM	<40
10^+	5644.04(5)	3589	2054.550(50)	13000±390	+32.1(5)	−10.2(5)	16(5)	+44(7)	+52(2);$E2$	RDM	<40
$9^{(+)}$	5792.07(4)	3589	2202.603(30)	2550±100	−34(3)	−4(3)	6(6)	+4(17)	−44(2);$M1$	0.00	
$(11)^+$	6279.69(11)	5247	1032.19(10)	2200±90	+30(3)	−12(3)	10(1)	+61(14)	+47(5);$E2$	0.00	
$(10)^-$	6376.06(8)	5792	(583.99)	(1400^{+1000}_{-400})[o]			0(9)	−27(10)		0.00	
		5247	1128.2(7)	(5000±600)[p]						RDM	<40
(10^-)	6721.09(9)	6376	345.24(20)	860±70[q]	+40(3)	0(3)	−6(1)			0.00	
		6280	(441.40)	≤100							
		5792	(929.02)	≤200							
		5644	(1077.05)	≤200							
		5247	1473.65(20)	390±40	+4(6)	−4(6)				0.00	
		5164	(1556.62)	≤150							
(12^+)	6769.50(19)	6280	489.81(15)	1200±50	−62(5)	+14(5)	12(5)	−5(7)	−71(5);$M1$	0.00	
$(11)^+$	6953.94(7)	5644	1309.830(70)	7960±240	−25.8(6)	−0.4(6)	0(4)	+32(4)	+34(1);$E1$	RDM	<40
(11^-)	7008.62(7)	6954	54.660(50)	450±50[r]	+76(16)		0.(4)			0.00	
		6721	287.546(60)	1800±50	−35(2)	0		−35(12)	−45(3);$M1$	0.00	
		5644	1364.73(20)	1320±50	−24(3)	−4(4)		+8(10)	−32(4);$M1$	0.00	
$(10)^+$	7025.58(7)	5792	1233.535(90)	(550±80)[s]	−29(4)	−1(4)	1(3)			0.00	
		5644	1381.78(30)	190±20	+8(20)	−19(30)				0.00	
		5247	(1778.07)	(1980±200)[t]	−22(3)	+2(2)		+33(10)	−30(3);$M1$		
		5164	1861.37(30)	530±25	+28(10)	−6(12)				0.00	
$(11)^+$	7194.32(7)	7026	168.760(4)	3080±100	−30(2)	0(2)	0(10)	−22(8)	+39(3);$M1$	RDM	<40
		6376	818.231(50)	6920±200	−26(3)	0(4)		+31(3)	+34(4);$E1$	RDM	
		5792	(1402.24)	<100							
		5644	1550.27(30)	350±30	−71(7)	−4(7)				0.00	
$(12)^+$	7223.88(7)	7194	29.566(70)	(11300±1600)[u]	−16(4)	0	44(12)			(RDM)	85(15)
		7009	215.273(40)	(3720±300)[v]	−37(9)	0				RDM	
		6954	269.931(50)	7850±250	−26(1)	0		+36(6)[m]	+33(3);$E1$	RDM	
		5644	1580.00(30)	200±20	+48(14)	−18(18)				0.00	
$(13)^+$	7437.82(8)	7224	213.930(40)	(17700±600)[w]	−32(2)	+2(2)	29(8)	−19(4)	−41(3);$M1$	RDM	4.2(7)
$(14)^+$	8058.39(11)	7438	620.576(70)	14800±440	−39(4)	0	33(7)	−15(2)	−49(5);$M1$	21(3)	0.4(2)
		7224	(834.50)	<200							
		6770	(1288.88)	<200							
$(15)^-$	8958.11(23)	8058	899.71(20)	9270±300	−34(2)	0	38(4)	+43(15)	+44(2);$E1$	21(3)	0.7(4)
		7434	(1520.28)	<100							
(16^-)	(9707.0(3))	8958	748.87(20)[x]	1600±80	−56(5)	0	16(1)	0(20)	−66(5);$M1$	40(4)	0.7(2)

TABLE III. (*Continued*).

J_i^{π}[a]	E_i[b] (keV)	E_f (keV)	E_γ[c,i] (keV)	Angular distribution[d,e] I_γ	A_2 (%)	A_4 (%)	I_f[f] ($\times 10^{-2}$)	$P(\%)$[g,e] expt	th	$F(\tau)$[h] (%)	τ (ps)
$(15)^+$	9836.0(3)	8058	(1777.6)[t]	[2230][t,y]	−22(2)	+ 2(2)	0(5)	+ 33(10)	−30(3);*M* 1		
$(16)^+$	10125.8(3)	9836	289.83(6)	2230±90	−25(3)	0	17(11)	−30(14)	−33(4);*M* 1	16(3)	0.9(3)
		8958	1167.70(20)	3900±160	−28(4)	0		+ 44(8)	+ 37(4);*E* 1	17(3)	
		8058	[2067.4]	< 200							
(17^+)	10764.9(8)	10125	639.04(70)[z]	4400±1000	−46(5)	0	6(15)	−17(7)	−53(8);*M* 1	44(5)	0.2(2)
		9836	(928.9)	< 250							
		8958	(1806.7)	< 200							
(18^+)	11403.9(11)	10765	639.04(70)[z]	3800±1000	−46(5)	0	18(11)	−17(7)	−53(8);*M* 1	44(5)	0.30(15)
		10126	(1278.1)	< 150							
(19^+)	12110.7(11)	11404	706.83(30)	2050±200	−80(60)	0	6(5)	+ 10(12)	−86(60);*M* 1	65(5)	0.20(7)
		10765	(1345.9)	< 200							
(20)	12964.7(12)	12111	854.00(30)	1400±400			14(4)	+ 40(20)		> 50	< 0.5
		11405	(1560.8)	< 150							
	unknown		134.34(3)[aa]	400±70	−3(12)	0				0.00	
	unknown		429.91(80)[aa]	1320±100	−33(4)	0		−25(8)	−42(4);*M* 1	0.14(3)	
	unknown		484.75(25)[aa]	2420±100	−17(10)	0		−4(7)	−24(14);*M* 1	0.26(4)	
	unknown		516.40(25)[aa]	940±100	−39(6)	0		−18(10)	−49(6);*M* 1	0.00	
	unknown		713.05(20)[bb]	1360±50	+ 12(4)	+ 5(4)		−22(19)	+ 19(7);*M* 1	0.00	

[a]See the text.

[b]Corrected for recoil. The uncertainty in the least significant figure is given in parentheses. E_i completely enclosed in parentheses are to some degree speculative.

[c]Not corrected for recoil. Energies enclosed in parentheses are calculated from $E_i - E_f$. Those in square brackets were not positively identified in the $\gamma\gamma$ coincidence data and thus are somewhat uncertain.

[d]The relative intensity I_γ is corrected for the relative γ-ray efficiency and is in arbitrary units. Intensities given in parentheses were extracted from unresolved multiplets using auxiliary information (excitation functions, coincidence data, etc). Intensities in square brackets were estimated. An entry of 0 for A_4 means the fit was to $I_\gamma(1+A_2P_2)$ only, i.e., χ^2 was not significantly improved by the inclusion of an A_4 term.

[e]In the case of unresolved doublets an attempt has been made to correct A_2, A_4, P, and $F(\tau)$ for the other member of the doublet unless otherwise footnoted. These corrections made use of all the ^{74,76}Ge + ^{18}O angular distribution, linear polarization, and excitation function data.

[f]Relative side feeding of the level in question in units of $100I_\gamma$.

[g]The linear polarization (see the text). The theoretical (th) value is calculated assuming the indicated pure multipole.

[h]The Doppler shift attenuation factor. [An entry RDM means $F(\tau)=0$ and τ was measured by the recoil distance method.]

[i]The E_γ and E_i for $E_i < 5.5$ MeV are from ^{90}Nb(β^+/EC)^{90}Zr (Ref. 11).

[j]The intensity balance was calculated using an internal conversion coefficient of 2.900 (see Ref. 11).

[k]Used for normalization of the angular distributions, i.e., assumed isotropic since $\tau = 1.17$ s (Ref. 10).

[l]Unresolved from the 6376→5247 1128-keV transition. I_γ(total) = 39000±1000. The angular distribution coefficients and linear polarization are for the doublet.

[m]Unresolved from the ^{87}Sr 3391→3249 transition. I_γ(total) = 2800±720. The ^{90}Zr angular distribution and linear polarization were estimated assuming $A_2 = -26(3)$ for the *M* 1 ^{87}Sr component. The intensity balance in ^{90}Zr was calculated with an internal conversion coefficient of 0.3184 (see Ref. 11).

[n]Triplet with ^{89}Y and ^{85}Sr. I_γ(total) = 10000±300.

TABLE III. (*Continued*).

[o]Triplet with ^{208}Pb and ^{89}Zr. I_γ(total)=3200±100. P and $F(\tau)$ are for the composite peak.
[p]Doublet with the 1129-keV 3448→2319 transition. E_γ was obtained from the average E_γ, the known 1129-keV energy (Ref. 11), and the relative intensities of the 1128- and 1129-keV transitions. I_γ(total)=39000±1000. The A_2, A_4, and P are for the doublet.
[q]There is a mismatch of 550±100 in I(in)−I(out). This could possibly be made up of contributions for which limits on the intensity are given.
[r]Calculated from an observed intensity of 275±30 using $\alpha(M1)=1.104$.
[s]Doublet with ^{88}Zr. I_γ(total)=860±50.
[t]The 7025→5247 and 9836→8058 transitions are degenerate with the ^{28}Si 1778→0 transition. I_γ(total)=4200±120. A_2, A_4, and P are for the composite peak.
[u]Doublet with ^{89}Zr. The total observed γ intensity was 2300±200 of which 1450±200 was assigned to this transition. The quoted I_γ was derived using $\alpha(M1)=6.813$ (see the text).
[v]Doublet with ^{89}Zr. I_γ(total)=5500±150.
[w]Doublet with ^{88}Y. I_γ(total)=21400±550.
[x]The placement is uncertain although the assignment to ^{90}Zr is not.
[y]The intensity is assumed to match that of the feeding intensity.
[z]The two 639-keV transitions are degenerate. The intensity balance is estimated from the $\gamma\gamma$ data. The angular distribution, linear polarization, and Doppler shift information are for the composite peak.
[aa]These transitions are most probably in ^{90}Zr; the placement is unknown.
[bb]There is some uncertain evidence from the $\gamma\gamma$ data that this γ transition is a 6376→5644 transition. However, E_γ and A_2, A_4, and P are in poor agreement with this placement (see the text).

tors faced each other across the axis of rotation which passes through the target position. The front faces of the detectors were 2.5-cm apart and their centers were 23 cm from the target. The detectors were partially shielded with lead so that only ~2.5 cm of the front segment of each was exposed to γ rays from the target. The mean angle of the detectors from the beam axis was determined by numerical integration to be 7° from the normal.[22]

The gains of the two detectors were adjusted to be approximately equal and a pulse-height spectrum was formed from a linear sum of the coincident events. A correction to the digitized signals was applied before summing to account for the fact that the gains were not exactly equal. The gains were inspected periodically during the measurements and the correction factor adjusted accordingly. The turntable was cycled between positions with the axis of symmetry of the detectors parallel (||) to the beam axis and, by a 90° rotation, perpendicular (⊥) to the beam axis. Both the singles and the summed spectra were collected "on line" in two different storage locations (|| and ⊥). The full cycle time, which varied with the count rate, was in the range 30—90 min. Data were collected for 24 h at $E(^{18}\text{O})=60$ MeV for both the ^{74}Ge and ^{76}Ge targets. A further measurement was made at $E(^{18}\text{O})=72$ MeV with the ^{76}Ge target.

The formalism used in the analysis of the linear polarization is that described by Poletti, Warburton, and Olness,[23] and only the major points are presented here. The degree of polarization at an angle θ_γ to the beam direction is defined as

$$P(\theta_\gamma)=\frac{[W(\theta_\gamma,0°)-W(\theta_\gamma,90°)]}{[W(\theta_\gamma,0°)+W(\theta_\gamma,90°)]}\ , \tag{5}$$

where $W(\theta_\gamma,\phi)$ is the probability of the emission of a γ ray from an aligned state at an angle θ_γ to the alignment axis (beam direction) and with the electric field vector at an angle ϕ to the reaction plane. If the γ ray is completely polarized in the reaction plane, then $P(\theta_\gamma)=+1$. Experimentally, one measures the quantity

$$S(\theta_\gamma)=\frac{(N_0-N_{90})}{(N_0+N_{90})}\ , \tag{6}$$

where N_0 and N_{90} are the areas under the photopeak of a given γ ray in the two polarimeter spectra accumulated with the interdetector axis parallel (||) and perpendicular (⊥) to the reaction plane, respectively. $P(\theta_\gamma)$ and $S(\theta_\gamma)$ are connected through the relation

$$P(\theta_\gamma)=S(\theta_\gamma)/Q\ , \tag{7}$$

where Q is a measure of the sensitivity of a system of finite detectors to linear polarization. Q is related to the asymmetry R, the ratio of the average cross sections for Compton scattering of the photon into directions parallel to and perpendicular to the polarization vector, by the expressions

$$Q=\frac{R-1}{R+1},\quad R=\frac{\bar{\sigma}_c(||)}{\bar{\sigma}_c(\perp)}\ , \tag{8}$$

where $\bar{\sigma}_c(||)$ and $\bar{\sigma}_c(\perp)$ are the cross sections for scattering parallel or perpendicular to the electric vector. Since

Compton scattering perpendicular to the electric field vector is preferred, $R<1$ and $Q<0$. The actual value of Q at a given γ-ray energy was estimated by numerical integration and checked by measurement of γ-ray transitions produced in the $^{18}O+{}^{74,76}Ge$ reactions. The calibration transitions chosen could be shown to be $E1$ or $E2$ multipolarities, with lifetimes short enough to rule out significant $M2$ or $M3$ contributions. A previous study by Butler *et al.*[24] had shown that the expression

$$Q=KQ_{KN} \tag{9}$$

gave a good representation of Q vs E_γ for a similar linear polarization spectrometer. In Eq. (9), Q_{KN} is the Klein-Nishina (KN) expression for the Compton scattering through 90° assuming a point scatterer and a point detector. Accordingly, a least squares fit of Eq. (9) to the calibration points was made as shown in Fig. 6. The resultant $K=0.72\pm0.03$ was used in the subsequent analysis. For mixed quadrupole-dipole transitions the linear polarization at 90° to the beam can be predicted from measured angular distribution coefficients by the formula[23]

$$P\equiv P(90°)=\pm\left[\frac{3(A_2+B_2)+\frac{5}{4}A_4}{1-A_2+\frac{3}{4}A_4}\right], \tag{10}$$

where B_2 is an analytical function of the quadrupole-dipole mixing ratio, of A_2, and of the initial and final spins of the transition. Since $B_2\equiv0$ for pure $L=1$ or 2 transitions and the A_ν are the usual Legendre polynomial expansion coefficients [Eq. (2)], the polarizations are easily calculated for pure multipole radiation. The plus sign applies for $M1$ or $E2$ radiation, and the minus sign for $E1$ or $M2$ radiation. Expressions for transitions involving higher order multipoles are given explicitly in Ref. 23.

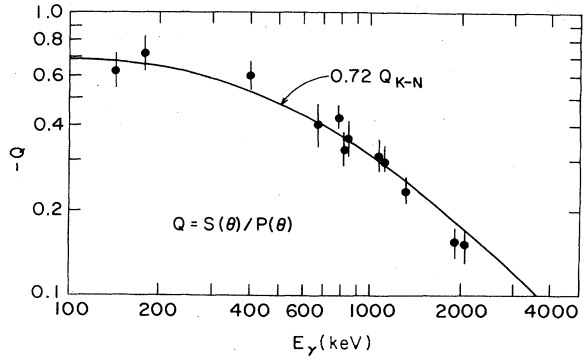

FIG. 6. Dependence of the polarization sensitivity parameter $(-Q)$ on the incident γ-ray energy E_γ. The experimental points were calculated from $E1$ and $E2$ γ transitions with measured angular distributions and therefore known polarizations. The curve is the Klein-Nishina expression [Eq. (2) of Ref. 23] scaled as indicated.

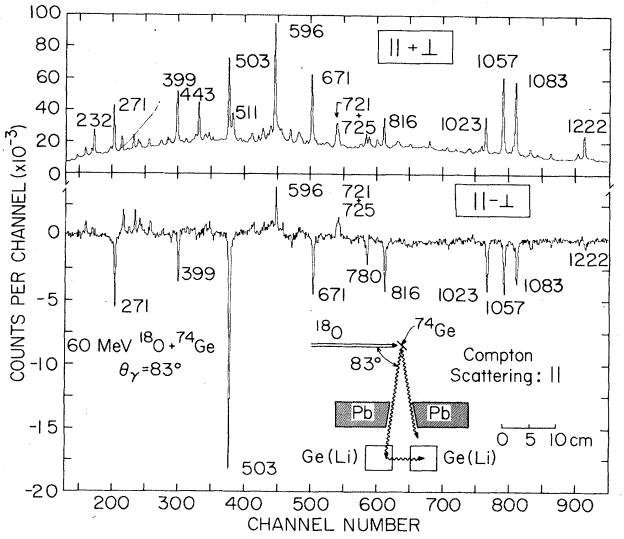

FIG. 7. Linear polarization results for $^{18}O+{}^{74}Ge$ at $E(^{18}O)=60$ MeV. The sum of the scattering in the reaction plane ($||$) and perpendicular to it ($\perp$) is shown in the top portion of the figure and the difference is shown in the bottom. With the convention used, stretched $E2$ transitions will have negative values of $||-\perp$ and stretched $M1$ transitions will have positive values.

Typical results are displayed in Fig. 7 which shows a portion of the linear polarization data for $^{18}O+{}^{74}Ge$. The linear polarization P for a given photopeak is formed by dividing its intensity in the lower part of the figure by that in the upper [Eq. (6)], and then dividing the resultant by Q. The values of P resulting from this procedure are listed in Tables II and III under "expt." The column marked "th" is the polarization calculated from Eq. (10) with $B_2=0$ for the indicated (pure) multipole (note, however, that the transition is not necessarily a pure multipole).

The linear polarization spectrometer described has an efficiency which falls off rapidly with decreasing E_γ for $E_\gamma\lesssim250$ keV, due to both the absorption of incoming and scattered radiation and the existence of an electronic cutoff. Thus, for instance, no polarization information was obtained with this arrangement on the important 85-keV 4798→4713 and 101-keV 4713→4612 transitions in ^{88}Zr. For this reason, a second experiment was performed using the LEPS and a planar Si detector at a distance such that the solid angles subtended were the same as in the first experiment. A 12-h run with a natural Ge target gave the results shown in Fig. 8. Since the 85- and 101-keV transitions have essentially identical $J+1\rightarrow J$ angular distributions (Table II), it is clear that they have different multipolarities. The 101-keV transition is $E1$ while the 85-keV transition is $M1$. The sensitivity of this low E_γ spectrometer was found to be the same as that predicted by $Q=0.72Q_{KN}$ if the 85- and 101-keV transitions were assumed to be pure multipoles.

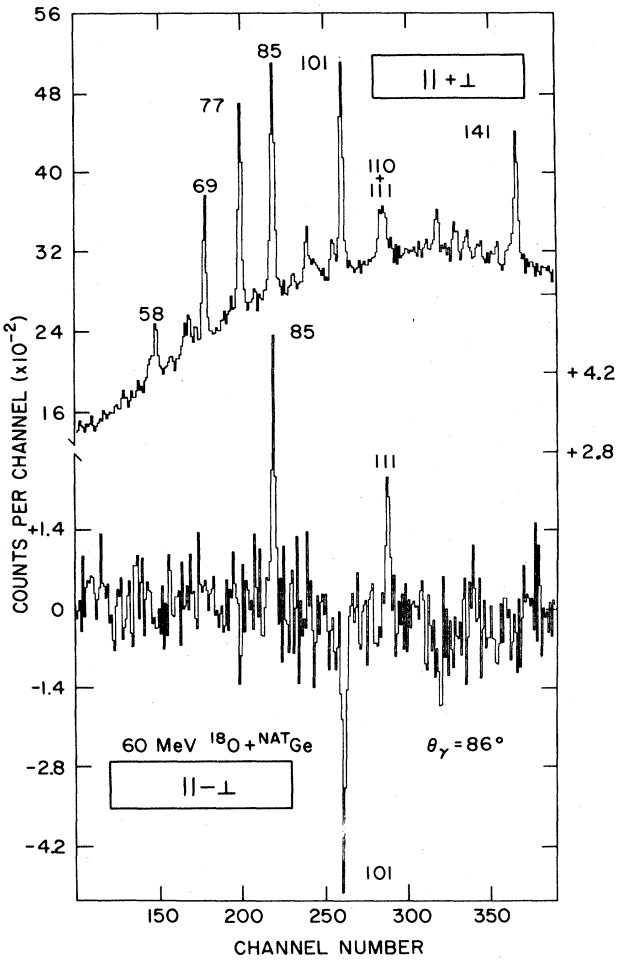

FIG. 8. Linear polarization results for $^{18}O+^{74}Ge$ at $E(^{18}O)=60$ MeV. From these results it is concluded that the 85- and 101-keV transitions have $M1$ and $E1$ character, respectively.

E. Gamma-ray recoil distance lifetime measurements

For this measurement targets were prepared by vacuum evaporation of Ge metals onto 2.5-mg/cm^2 Ta foils, which had been previously stretched over a ring holder to form a flat surface 6 mm in diameter. Although Ge metal is very brittle, and some difficulty was experienced in making uniform targets thicker than 100 μg/cm^2, a 550-μg/cm^2 target of natural Ge was eventually prepared after some considerable experimentation. Since ^{74}Ge is 36.4% abundant, the equivalent isotopic thickness for ^{74}Ge was 200 μg/cm^2. The purchased quantity of the separated isotope did not allow for such trial and error, and only a 60-μg/cm^2 target of ^{76}Ge was made. Both targets were examined with a microscope at 100 times magnification. They appeared quite uniform and were subsequently found to be stable under bombardment.

The targets were positioned in a holder which was translated relative to a fixed beam stop. Defining the target-stopper distance as D, the $D=0$ reading was determined by the touch point (zero electrical resistance). Two sets of runs were made for each target over the range $0 \le D \le 25\,000$ μ. As a precaution, the measurements for close distances ($D < 100$ μ) were made under manual control, while those for $D > 100$ μ were under automatic control. The step size was chosen so that the logarithmic change was constant with a given D about 60% larger than the next smaller one. Gamma rays were detected simultaneously by a coaxial Ge detector at $\theta_\gamma=0°$ and 8 cm from the beam stop and a LEPS at $\theta_\gamma=45°$ and 5 cm from the beam stop. Some data were also taken with the positions of the two detectors interchanged. An initial run used a ^{208}Pb beam stop to minimize general background, and a second run was made with an Au beam stop to study specifically the ^{88}Zr 85-keV transition which was completely masked in the initial run by the much stronger Pb $K\beta$ x rays. In general, the off-axis (45°) data provided a second set of data with flight peaks corresponding to a lower v/c, which proved useful in extracting some doublet structures which were unresolved in the on-axis data. All measurements were made with $E(^{18}O)=66$ MeV with the Ta backing facing the beam. Allowing for the energy loss in the Ta, this resulted in $E(^{18}O)\simeq 60$ MeV in the Ge target. The beam currents were ~ 12 nA for the natural Ge target and ~ 30 nA for the ^{76}Ge target, both resulting in a count rate ~ 10 kHz in the Ge detector.

The RDM relies on the fact that γ rays emitted at an angle θ_γ to the beam by nuclei recoiling with velocity v ($\equiv \beta c$) will have an energy given by Eq. (4) and thus the flight peak (I_s) can usually be separated from the stopped peak (I_0) arising from γ rays of energy $E_{\gamma 0}$ emitted by nuclei at rest. Since $D=vt$, the fraction of γ rays emitted by the target and surviving a flight path D to decay at rest in a beam stop is, to first order,

$$I_0/(I_0+I_s)=\exp(-D/v\tau)\,, \tag{11}$$

where τ is the mean life associated with the decay. The generalization to dependence on more than one lifetime is straightforward[25] and was made when appropriate (see the following).

In the analysis of the RDM results, the various corrections[25] to first order [Eq. (11)] were made to sufficient accuracy so that the uncertainties are generally dominated by the statistical and systematic errors in extracting the peak intensities. However, for the short mean lives, major uncertainties involve the absolute value of D and the feeding time due to cascades via higher-lying levels.

Both the DSAM and RDM information were acquired from singles data on γ-ray Doppler shifts. In determining the mean life (τ) of a given level, it was necessary, therefore, to take explicit account of the lifetimes (τ_i) and feeding fractions (F_i) of those states deexciting to the state of interest. Here, F_i specifies the fractional feeding (in %) via the ith level of mean life τ_i. The normalization is such that the direct feeding (assumed to be negligibly fast) is then given as $I_f=100-\Sigma_i F_i$. Values of I_f are given in Tables II and III. Clearly, for cases where $\tau_i \ll \tau$, the effect of such feedings F_i is negligible. However, for $\tau_i \sim \tau$, this feeding must be taken into account, as is discussed for the DSAM and RDM analyses which follow.

The peak-fitting code SAMPO was used to determine the relative intensity of the stopped peak I_0 as a function of target-stopper distance D. Most of the data were analyzed using Eq. (11) and the intensities of only the stopped peaks, i.e., $I_0+I_S=N_0=$constant. For some stronger transitions it was possible to extract the intensity of the flight peak I_S also, and thus create as a function of D the ratio $R\equiv I_0/(I_0+I_S)$ of Eq. (11). This latter procedure has the advantage that for $D=0$ we must also have $R\equiv 1.0$. These results provided a satisfactory check that the "zero distance" determined by electrical contact was sufficiently accurate for the analysis that ensues. For all cases, the distance dependence of I_0 was normalized (to $\pm 7\%$) according to the integrated beam currents for each run. Final normalization was based primarily on the distance-independent values of I_0 for long-lived ($\tau > 1$ ns) transitions. Addition checks were obtained for stronger transitions from the sums I_0+I_S. The overall normalization obtained in this manner was good to about $\pm 3\%$. The resultant determinations of τ are summarized in Tables II and III, and identified by the origin of the results as RDM in the $F(\tau)$ column.

F. Synthesis of results

1. Basic ground rules and assumptions

The purpose of the angular distribution and linear polarization measurements is to allow the extraction of information on spin-parity assignments and multipole mixing ratios. In this we also rely on knowledge of the reaction mechanism and the lifetime determinations. The fusion-evaporation reaction mechanism is well known and follows rather general systematic behavior while semirigorous upper limits to transition strengths can be invoked to limit the possible multipolarities. For the purpose of identifying γ-ray multipolarities the following rules and assumptions will be called upon as R1, R2, etc.

(1) The maximum orbital momentum brought into the compound systems $^{18}O+{}^{74,76}Ge$ at $E(^{18}O)=60$ MeV is, from semiclassical arguments, $\sim 30\hbar$, and from accumulated systematics we expect to form yrast states up to $\sim 20\hbar$ in $^{88,90}Zr$. A calculation with CASCADE (Ref. 19) gave $J=14\hbar$ (FWHM $\sim 13\hbar$) as the most probable spin formed in ^{90}Zr at the peak of the excitation function for $^{76}Ge+{}^{18}O$. We find that fulfillment of this prediction is possible only if essentially all observed transitions have $J_i \geq J_f$.

(2) The alignment of the yrast states in $^{88,90}Ze$ will be high. Defining the alignment parameters α_K by[27]

$$W(\theta_\gamma)=\sum_{K\ \text{even}} \alpha_K A_K^{\max} P_K(\theta_\gamma)\ , \tag{12}$$

where $A_K^{\max}$ is the angular distribution coefficient for complete alignment, then we expect[27-30] $\alpha_2=0.4$—0.9, and $\alpha_4 \simeq 0.2$—0.8.

(3) The mechanism for direct feeding of the levels of Figs. 3 and 4 is evaporation of neutrons followed by emission of several continuum γ rays. Since this latter process preserves alignment (the U_K coefficients[27] of intermediate transitions are ~ 0.98), the assumption can be made that the alignment is essentially the same for direct feeding of all levels. For the same reason, feeding from higher-lying observed levels (cascade feeding) has only a small effect on the alignment and this effect can be calculated from the known decay scheme.

(4) We follow the recommended upper limits (RUL) of Endt[31] for the maximum strength of any multipole. These upper limits in Weisskopf units[32] (W.u.) are as follows:

Multipolarity	RUL
$E1$	10^{-2}
$E2$	300
$E3$	100
$M1$	3
$M2$	1
$M3$	10

(5) Some general statements based on R1—R4 can be made about the transitions of interest. All transitions for which a lifetime was measured are dipole or $E2$ and many must be at least partially dipole (R4). All others, we assume, are at least partially dipole or quadrupole. This assumption is based on the many possible decay modes. Most transitions must have $J_i > J_f$ (R1). A weaker argument in favor of the dominance of $J_i > J_f$ is the general lack of crossover transitions other than those expected to be $E2$ (Figs. 3 and 4).

(6) Some general statements can be made for the behavior of γ transitions between high spin states (R2) (Refs. 27 and 33) assuming only $\alpha_K > 0$, $K=2,4$.

(a) Pure $J\pm 2\rightarrow J$ transitions have $a_2 > 0$, $a_4 < 0$.

(b) $J\pm 1\rightarrow J$ transitions have $a_4 \geq 0$ for all mixing ratios.

(c) $J\rightarrow J$ transitions have $a_4 \leq 0$ for all mixing ratios.

(d) In the high spin limit, there is a basic ambiguity between $J+2\rightarrow J$ and $J-2\rightarrow J$ $E2$ transitions and between pure $E2$ $J\pm 2\rightarrow J$ transitions and mixed $M1$, $E2$ $J\rightarrow J$ transitions with mixing ratio[34] $x\simeq -0.45$. This pertains to both angular distributions and linear polarization data.[35] However, for small enough spin values the linear polarization can be invoked to resolve the latter ambiguity. Thus, it is often possible to fix the often encountered $J+2\rightarrow 2$ transitions as such (using R6a—c) without recourse to any assumptions about the reaction mechanism other than $\alpha_K > 0$, $K=2,4$.

2. Applications

The first step in the analysis was to establish the more intense $J+2\rightarrow J$ transitions as such and to use them to calibrate the α_K's. These could then be applied to the determination of mixing ratios for $J\pm 1\rightarrow J$ and $J\rightarrow J$ transitions and to distinguishing between these three types of transitions.

The transitions considered are the $4413\rightarrow 3391$ and $5229\rightarrow 4413$ transitions in ^{88}Zr (Fig. 3) and the $5644\rightarrow 3589$ and $6280\rightarrow 5247$ transitions in ^{90}Zr (Fig. 4). For these transitions, the angular distributions (Tables II and III) rule out both $J\pm 1\rightarrow J$ transitions (R6b) and $J-2\rightarrow J$ transitions (e.g., $|A_4| \leq 0.06$ for these $E2$ transitions with $J=8$, 9, and 10). For $J\rightarrow J$ the predicted po-

larization at the "solution" (R6d) near $x=-45°$ is $\sim\frac{1}{2}$ of the measured polarization for all four transitions and $\gtrsim 3$ standard deviations away. Thus, $J+2\rightarrow J$ for all four transitions. The α_K's were then calculated from a least squares fit to the four values derived from

$$\alpha_K = A_K(\text{exp})/A_K^{\max} . \tag{13}$$

They were in excellent agreement, and we found $\alpha_2=0.83$, $\alpha_4=0.58$. An uncertainty of 0.05 was assigned to each to cover the spread expected from differences in the feeding of the various levels by the multineutron xn evaporation process. Note that these α_K's include the effect of the finite solid angle subtended by the γ-ray detectors. The α_K results are in accord with expectations from systematics for similar heavy ion reactions.

The analysis for a given transition proceeded as follows: With J_i and J_f assumed, arctan$x$, with x the $(L+1)/L$ mixing ratio, was varied in 1° steps from $-90°$ to $+90°$. For each value of x, the theoretical angular distributions were calculated from

$$W(\theta_\gamma)_{\text{th}} = \sum_K \alpha_K A_K^{\max}(\text{th}) P(\theta_\gamma)$$
$$= \sum_K A_K(\text{th}) P(\theta_\gamma) , \tag{14}$$

where $A_K^{\max}$(th) is a known[27] function of J_i, J_f, x, and, within coarse limits, the α_K's were corrected for the difference in cascade feeding between the transition being considered and the calibrating transitions. In addition, the polarization was calculated from Eq. (10) using (a) the experimental A_2, A_4 values and (b) the theoretical A_2, A_4 values. Let us call these $P_{\text{th}}^{(a)}$ and $P_{\text{th}}^{(b)}$. Then, χ^2 was formed according to

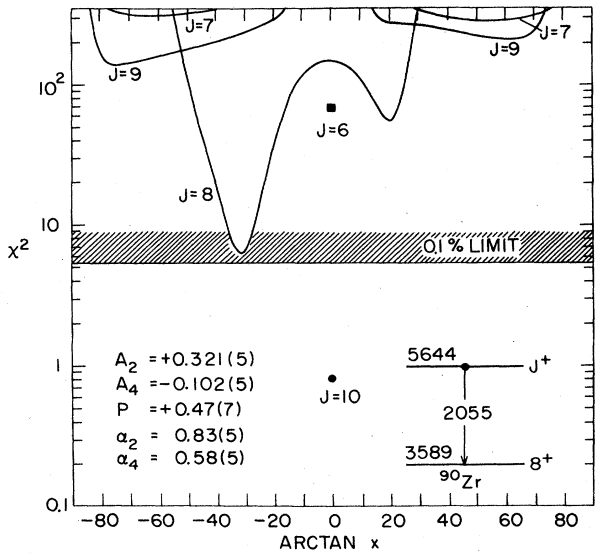

FIG. 9. χ^2 vs arctan$x$ curves for the ^{90}Zr 5644→3589 transition. The curves are based on the indicated parameters. The curves for $J^\pi=7^-$, 8^-, and 9^- are all above $\chi^2=119$, 24, and 83, respectively.

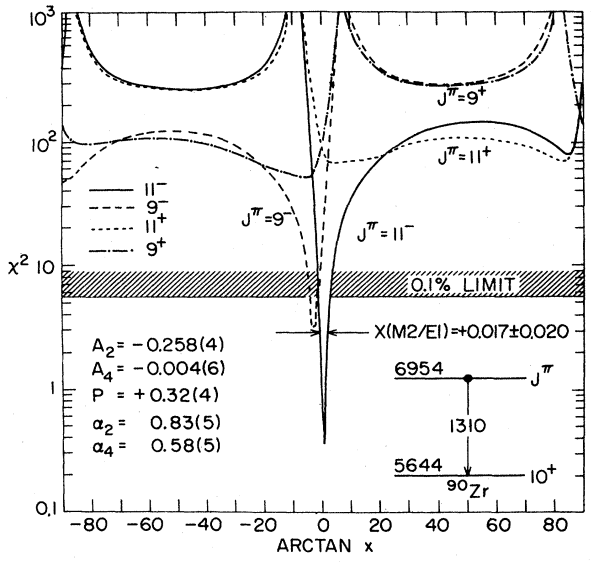

FIG. 10. χ^2 vs arctan$x$ for the ^{90}Zr 6954→5044 transition. The curves are based on the listed parameters. The χ^2 values for the $E2$ $12^+\rightarrow 10^+$ and $8^+\rightarrow 10^+$ transitions are 377 and 421, respectively. For $10^\pm\rightarrow 10^+$, χ^2 is everywhere >57.

$$\chi^2 = \frac{(P-P_{\text{th}})^2}{3(\Delta P)^2} + \frac{[A_2-A_2(\text{th})]^2}{3(\Delta A_2)^2} + \frac{[A_4-A_4(\text{th})]^2}{3(\Delta A_4)^2} , \tag{15}$$

where the uncertainties $(\Delta P, \Delta A_K)$ are composed of the uncertainties in the experimental and theoretical values added in quadrature and the larger of $(P-P_{\text{th}}^{(a)})^2$, $(P-P_{\text{th}}^{(b)})^2$ was chosen. This is not a rigorous definition; however, it is a reasonable prescription and we found it to provide a sound quantitative value of χ^2 for distinguishing between solutions. An example of its use is shown in Fig. 9 which is a χ^2 vs arctan$x$ curve for the ^{90}Zr 2055-keV 5644→3589 transition used as one of the calibrator transitions of the α_K's. The reasons for the unacceptable fits for the $J\pm 1\rightarrow J$ and $J-2\rightarrow J$ possibilities have been discussed in the text. Of course, for the α_2, α_4 variable the rejection of $J_i=6-9$ would not be so clean. For instance, the best $J_i=8$ solutions occurs for $\alpha_2=\alpha_4=1.0$ (however, it is still not acceptable).

An example of a fit to the $J+1\rightarrow J$ transition is shown in Fig. 10. This example illustrates the ability to distinguish a pure dipole $J\pm 1\rightarrow J$ transition from $J\rightarrow J$ and $J\pm 2\rightarrow J$ and also to fix it as $E1$ or $M1$.

III. RESULTS

A. ^{88}Zr

1. *Lifetime measurements*

DSAM. Curves of $F(\tau)$ vs τ were generated using a computer code based on the Blaugrund[26] representation of nuclear scattering. The code allows explicitly for the in-

clusion of a single effective feeding fraction F_1 and lifetime τ_1. More complex cases were dealt with in an approximate way by using an effective F_1,τ_1 due to two or more sets of F_i,τ_i. A 15% uncertainty was assigned to the stopping power of the target and backing.

We now consider briefly the resultant solutions for $F(\tau)$ and τ given in Table II. First, no cascade feeding is observed into the 11200-keV level, and hence, $F_1=0$. The observed attenuation factor then leads directly to the result $\tau=0.32(14)$ ps as a composite lifetime for the state and feeding. For the 10577-keV level, because the DSAM results are dominated by feeding from the 11200-keV level [$F_1=65(33)\%$] and also the experimental $F(\tau)$ is itself not well determined, we obtain only the upper limit $\tau\leq 0.2$ ps. For the 9913-keV level no shift is observed [$F(\tau)=0(1)\%$] and we obtain correspondingly a lower limit $\tau>1.0$ ps. A limit is obtained for the 8925-keV level while for the 8200-keV level the apparent lifetime is only slightly longer than the major feeding branches, and we obtain a definite, but poorly determined, value for τ. For the next four lower levels, on the left-hand side of Fig. 3, we have $48\leq F_i\leq 100\%$, and we obtain only lower limits for the lifetime of the levels in question. Nevertheless, these limits are sufficiently fast as to rule out pure quadrupole radiations, and thus they determine that spin changes are restricted to $\Delta J\leq 1$ for all transitions on the left-hand side of Fig. 3 from levels with $E_x>6.5$ MeV except the 9913-keV level.

From similar analyses we arrive at the results tabulated for the levels involved in the cascade sequence beginning with the 7432-keV level and ending at the 5229-keV level (i.e., the right-hand side of Fig. 3). Again, the relatively fast lifetimes determine that these are all predominantly dipole transitions ($\Delta J\leq 1$) with the exception of the weak 6239→5229 transition.

RDM. Figure 11 shows RDM data on the cascades of γ rays from the 6193- (upper plot) and 5229-keV (lower plot) levels of ^{88}Zr. (The feeding parameters and lifetimes are those given in Table II.) The RDM decay curves for the 1395- and 609-keV γ rays are in agreement and lead to a meanlife for the 6193-keV level of $\tau_1=2.45(20)$ ps. For the 5584-keV level, the I_0 vs D decay curve is indistinguishable from that shown for the decay of the 6193-keV level which feeds it via the 609-keV transition. Thus we conclude that $\tau(5584)\ll\tau(6193)$. In fact, from the DSAM analyses we have already concluded that $\tau(5584)<1$ ps.

In the lower portion of Fig. 11 we show a fit to the decay of the 817-keV line from the 5229-keV level, which leads to the result $\tau(5229)=15(1)$ ps. Again, the decay curve for the subsequent 1023-keV line merely reflects the lifetime of this 5229-keV level, and we obtain only the limit $\tau(4413)<2$ ps. (Note that a contribution from long-lived background due to ^{87}Y has been subtracted for this data on the 1023-keV line.) Figure 12 shows data on this cascade 4798→4713→4612 keV. The ~2.5-ps feeding into the 4798-keV level is so short as to introduce only a small perturbation into the analyses of the 85-keV γ-ray decay curve, which yields the result $\tau(4798)=72(6)$ ps. The lower curve shows the results of a two-lifetime fit to the data on the 101-keV line, which yields the result

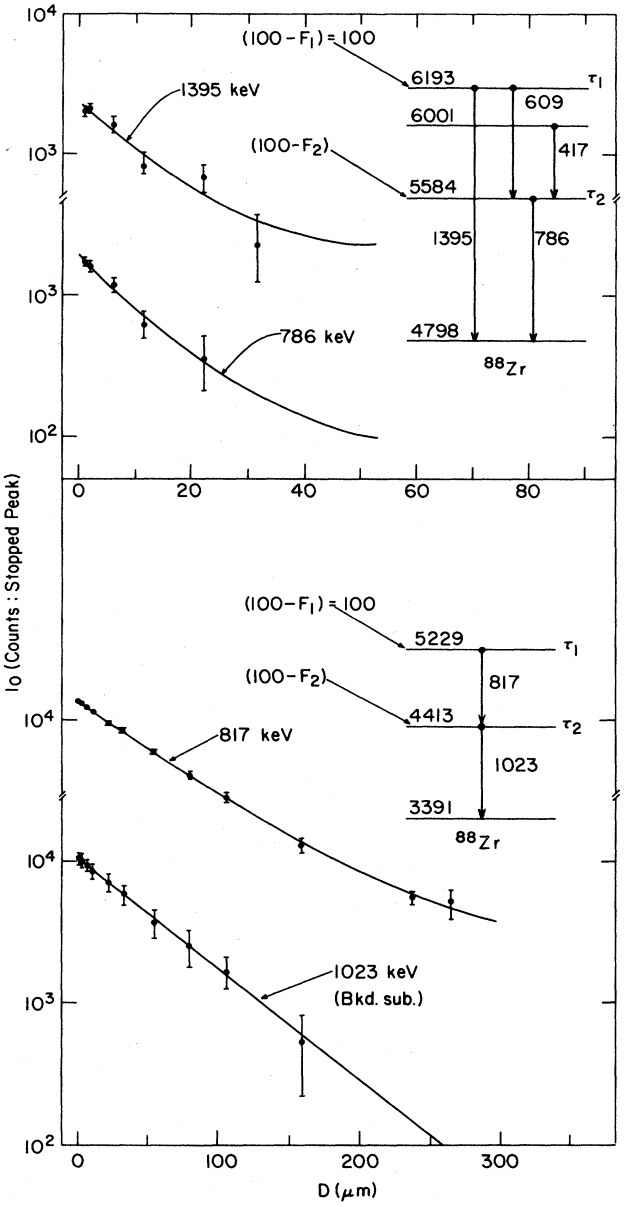

FIG. 11. Recoil distance lifetime results for the 6193-, 5584-, 5229-, and 4413-keV levels of ^{88}Zr. The results are discussed in the text.

$\tau(4713)=3250(250)$ ps. The effect of the 72-ps feeding from the 4798-keV level is easily seen as a flattening of the decay curve in the region $D<5$ mm.

The lifetime data on the 3391-keV level is shown in Fig. 13. The 3391-keV level is fed almost totally via two different cascades routes involving markedly different feeding lifetimes: the decay curve for the 503-keV γ ray is thus the simple sum of the decay curves that pertain individually to the two routes. The 3250-ps feeding dominates the decay for distances $D>2$ mm and this portion of the data is well fitted for the lifetime of the 4612-keV level. For $D<2$ mm the curve is determined by the life-

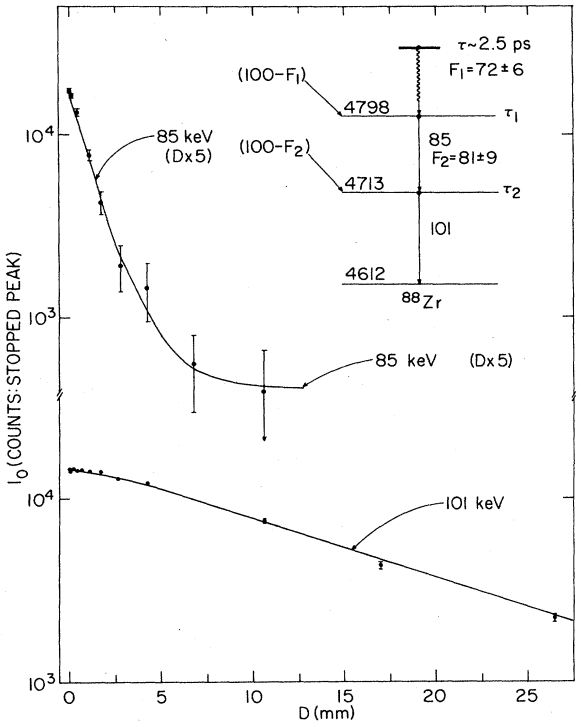

FIG. 12. Recoil distance lifetime results for the 4798- and 4713-keV levels of ^{88}Zr. The results are discussed in the text.

time of the 3391-keV level and the 15-ps feeding from the 4413-keV level. A fit to these data determine $\tau(3391)=30(2)$ ps.

2. *Synthesis of results*

Here we consider ^{88}Zr level by level starting with the first level above the 2888-keV 8^+ isomer. The properties of the isomer and levels below it are taken as determined by previous investigations.[9,13,14] Note, however, that for these levels the data summarized in Table II are consistent with previous spin-parity and multipolarity assignments and in some cases are an independent determination of them. In Table IV we give a summary of the results from a simultaneous analysis of the angular distribution, linear polarization, and lifetime data of Table II. This table supplements the following discussion.

The 3391-keV level. This level is formed in ^{88}Nb(β^+/EC) with an allowed logft value of 5.6.[11] The accepted criterion for assigning allowed decay for $Z<80$ is log$ft<5.9$;[36] hence, $\Delta J=0,\pm1$ with no change of parity. Accepting $J^\pi=8^+$ for the ^{88}Nb ground state[9] allows $J^\pi=7^+$, 8^+, and 9^+ for the ^{88}Zr 3391-keV level. As illustrated in Fig. 14, the present angular distribution and linear polarization results rule out the 7^+ and 9^+ alternatives and leave a definite $J^\pi=8^+$ assignment with $x(E2/M1)=0.15(7)$ for the 3391→2888 transition. This assignment is in agreement with previous fusion evaporation results,[13,14] based on angular distributions alone.

The 4413-keV level. The 1022-keV 4413→3391 transition is characteristic of a stretched $E2$ transition with values of A_2, A_4, and P (and hence χ^2 vs arctan$x$ curves) essentially the same as the ^{90}Zr 2055-keV 5644→3589 transition (see Fig. 9). A $10^+\xrightarrow{E2}8^+$ assumption yields the acceptable χ^2 value of 1.3. For a $J^\pi=8^+$ assignment to the 4413-keV level the minimum χ^2 is 5.8 and occurs for arctan$x=16°$; while a $6^+\xrightarrow{E2}8^+$ assumption yields $\chi^2=5.0$. The reasons for these latter two poor fits have been discussed (Sec. II F 2). A 10^+ assignment is also favored by the reaction mechanism (R1) as follows: The 4413- and 4612-keV levels were formed in the (α,2n) stud-

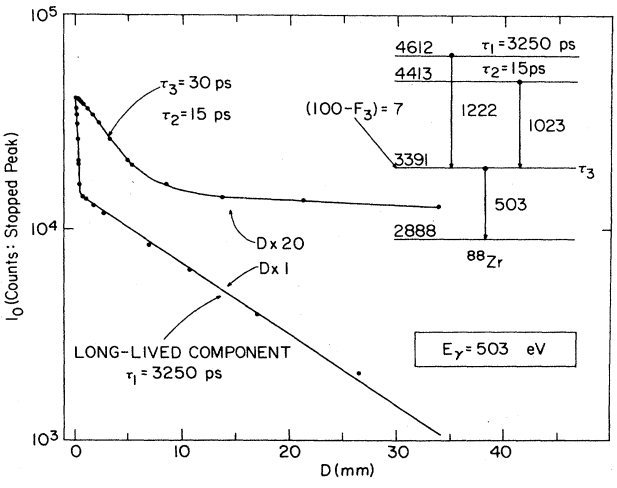

FIG. 13. Recoil distance lifetime results for the 3391-keV level of ^{88}Zr. The results are discussed in the text.

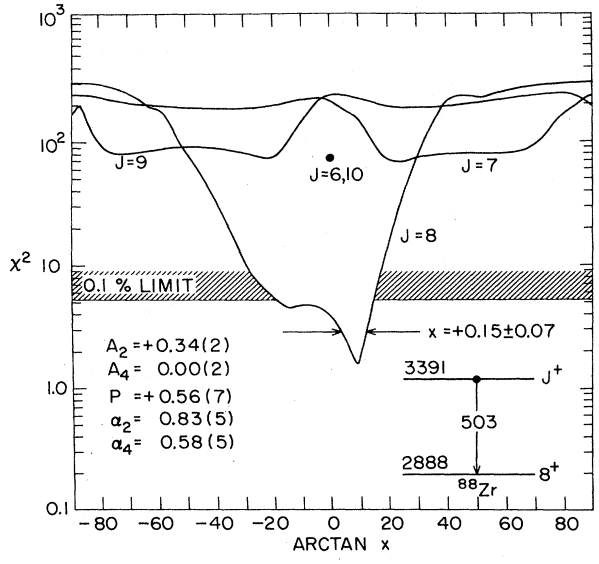

FIG. 14. χ^2 vs arctan$x$ for the ^{88}Zr 4612→3391 transition. The curves are derived from the listed parameters. The χ^2 values for pure $E2$ $10^+\to8^+$ and $6^+\to8^+$ transitions are 395 and 372, respectively. The $J_i^\pi=7^-$ and 8^- curves have χ^2 values everywhere above 7.2 and 170, respectively.

TABLE IV. ^{88}Zr branching ratios, partial lifetimes, mixing ratios, and transition strengths.

E_i (keV)	E_f (keV)	E_γ (keV)	Branching ratio[a] (%)	τ(partial)[b] (ps)	Dominant multipole	$x(L+1/L)$[c]	$B(L)$[d] (W.u.)	$B(L+1)$[d] (W.u.)	Conclusions and remarks
3391	2888	503	100	30(2)	$M1$	+0.15(7)	$8.1(6)\times10^{-3}$	0.8(6/9)	$J\rightarrow J;M1$ (see the text)
4413	3391	1022	98.2(3)	>2	$E2$		>15.42		$J+2\rightarrow J;E2$ (see the text)
	2888	1525	1.8(3)	>95	$E2$		>0.038(5)		
4612	4413	199	1.8(5)	$<13.9\times10^3$	$M1$	+0.2(9/3)			
	3391	1222	94.4(9)	<265	$M1$	+0.68(36/21)[e]	$>0.045(9/13)\times10^{-3}$	>0.015(11/7)	$J\pm1\rightarrow J;M1$ (see the text)
	2888	1724	3.8(8)	$<6.6\times10^3$	$M1$	−0.05(8)[e]	$>9.4(20)\times10^{-7}$	>5.6(27/4)	$J\pm1\rightarrow J$[f]
4713	4612	101	78(2)	$4.63(70)\times10^3$	$E1$	+0.02(4)[e]	$0.10(1)\times10^{-3}$	18(2/165)	$J\pm1\rightarrow J;E1$[f]
	4486	227	16(2)	$2.0(3)\times10^4$	$M1$	+0.09(5)[e]	$0.13(2)\times10^{-3}$	0.02(2.3)	See the text
	4413	300	6(1)	$5.4(10)\times10^4$	$E1$	−0.15(45)[e]	$3.6(5/10)\times10^{-7}$	0.4(10/45)	See the text
4798	4713	85	88(1)	109(9)	$M1$	+0.02(6)[e]	0.48(5)	30(90/450)	$J\pm1\rightarrow J;M1$[f]
	4413	385	12(1)	600(70)	$E1$	+0.03(4)[e]	$0.014(2)\times10^{-3}$	0.4(4/18)	See the text
5229	4413	816	100	15(1)	$E2$		6.45(43)		$J+2\rightarrow J;E2$[f]
5666	5229	436	100	0.40(15)	$M1$	<0.16[g]	0.95(14)	$5.5(21)\times10^3$[h]	
5951	5666	285	3.7(4)	<3.7	$M1$	<0.14[g]	>0.58	$>5.0\times10^3$[h]	$J\pm1\rightarrow J;M1$[f]
	5229	721	96.3(4)	<0.16	$M1$	<0.30[g];+0.07(4)[e]	>0.54	$>1.1\times10^3$[h]	$J\pm1\rightarrow J;M1$[f]
6239	5951	288	82.3(9)	1.8(5)	$M1$	<0.11[g]	0.73(20)	$9.8(27)\times10^3$[h]	$J+1\rightarrow J;M1$[f]
	5229	1009	17.7(9)	8.5(23)	$E2$	[0]	4.0(11)		
6501	5951	551	100	0.23(5)	$M1$	<0.20[g];+0.00(5)[e]	0.83(18)	$3.0(7)\times10^3$[h]	$J+1\rightarrow J;M1$[f]
6827	6501	325	25.1(13)	0.60(12)	$M1$	<0.09[g]	1.54(32)	$1.6(3)\times10^4$[h]	$J\pm1\rightarrow J;M1$[f]
	6239	588	74.9(13)	0.20(4)	$M1$	<0.22[g]	1.40(28)	$2.5(5)\times10^3$[h]	$J\pm1\rightarrow J;M1$[f]
7432	6827	605	100	0.15(4)	$M1$	<0.21[g]	0.95(25)	$2.9(8)\times10^3$[h]	$J\pm1\rightarrow J$
5584	4798	786	100	<1.0	$M1$	+0.00(4)[e]	>0.06	>116[h]	$J\pm1\rightarrow J;M1$[f]
6001	5584	417	100	<1.0	$M1$	<0.19[g];+0.07(12)[e]	>0.43	>2760[h]	$J\pm1\rightarrow J;M1$[f]
6032	4798	1234	100			>−0.09[e]			
6193	6032	160	9.3(9)	26.3(33)		<0.09[g];+0.08(8)[e]	0.29(4)	$1.26(15)\times10^4$[h]	$J\pm1\rightarrow J$; from A_2,τ
	5584	609	32.0(15)	7.66(72)	$M1$	+0.05(14)[e]	0.018(2)	55(5)[h]	$J\pm1\rightarrow J;(M1)$[f]
	4798	1395	58.7(17)	4.17(36)	$E2$			1.59(14)[h]	$J\pm2\rightarrow J;E2,J\rightarrow J;M1$
6765	6193	572	100	≤0.70	$M1$	<0.35[g];+0.16(7)[e]	≥0.24	≥800[h]	$J\pm1\rightarrow J;M1$[g]
7228	6765	463	100	≤1.1	$M1$	<0.26[g];−0.01(5)[e]	≥0.29	≥1500[h]	$J\pm1\rightarrow J;M1$[f]
7536	6765	771	100	≤0.48		0.00(12)[e]	≥0.14	≥265[h]	$J\pm1\rightarrow J$[g]
7879	7536	342	54(7)	≤1.5	$M1$	<0.14[g];+0.05(9)[e]	≥0.53	≥4970[h]	$J\pm1\rightarrow J;M1$[f]
	7228	651	46(7)	≤1.8	$(M1)$	+0.14(40/20)[e]	≥0.06	≥167[h]	$J\pm1\rightarrow J;(M1),(J\rightarrow J;M1)$

TABLE IV. (*Continued*).

E_i (keV)	E_f (keV)	E_γ (keV)	Branching ratio[a] (%)	τ(partial)[b] (ps)	Dominant multipole	$x(L+1/L)$[c]	$B(L)$[d] (W.u.)	$B(L+1)$[d] (W.u.)	Conclusions and remarks
8200	7879	321	100	0.4(6/2)	$M1$	<0.10[e]; $+0.00(3)$[e]	2.4(2.4/1.5)	2.6(25/15)$\times 10^4$[h]	$J\pm1\rightarrow J;M1$[f]
8925	8200	724	100	<0.5	$M1$	$+0.09(14)$[e]	>0.17	>150[h]	$J\pm1\rightarrow M1$[f]
9913	8925	987	48(5)	>1.9		$+0.11(16)$[e]	<0.02	<20[h]	$J\pm1\rightarrow J$[f]
	8200	1713	52(5)	>1.7				<1.4[h]	$J\pm2\rightarrow J,J\rightarrow J;M1$[f]
10577	9913	645	100	≤ 0.2		<0.25[g]	≥ 0.59	≥ 1570[h]	$J\pm1\rightarrow J;J\rightarrow J$[g]
11200	10577	642	100	0.32(20)	$(M1)$	<0.56[g]; $+0.25(85/35)$[e]	0.37(63/14)	1.0(17/14)$\times 10^3$[h]	$J\pm1\rightarrow J;(M1);J\rightarrow J;M1$

[a]The γ branching in percent.
[b]From the branching ratio and the level lifetimes of Table II. The lifetime is for the γ transition only, i.e., a correction has been made for internal conversion when significant.
[c]The $E2/M1$ or $M2/E1$ mixing ratios (amplitudes) from analysis of the angular distribution and linear polarization measurements together with any restrictions imposed by the measured partial lifetimes and the RUL (see the text). Values in brackets are assumed. The sign convention is that of Ref. 34.
[d]The transition strengths (in W.u.) of the lowest allowed multipole (L) and next-lowest allowed multipole ($L+1$) from τ(partial) and $x(L+1/L)$.
[e]For $J+1\rightarrow J$.
[f]From A_2, A_4, and P.
[g]From the partial lifetime and the RUL's. The limit is for the absolute magnitude.
[h]For $J\pm2\rightarrow J$.

ies[13,14] of ^{88}Zr, while only the 4612-keV level was formed in the p,2n reaction.[13] From this, one can argue that $J(4413)>J(4612)$ with the consequence that the $4413\rightarrow3391$ transition is not $J-2\rightarrow J$ (see Fig. 3 and the following). We conclude that the 4413-keV level can be given a definite $J^\pi=10^+$ assignment.

The 4612-keV level. Fits to the 1222-keV $4612\rightarrow3391$ transition are shown in Fig. 15. These fits establish the transition as $9^+\rightarrow8^+$ or $7^+\rightarrow8^+$. The properties of the various low-energy transitions connecting the final states between 4400 and 4800 keV (see Fig. 3) do not allow the spins of the 4413- and 4612-keV levels to differ by three units; hence, a definite $J^\pi=9^+$ assignment can be made to the 4612-keV level with $x(E2/M1)=+0.68(36/21)$ for the $4612\rightarrow3391$ transition in agreement with the previous tentative results[13,14] and expectations from the reaction mechanism. Although the $4612\rightarrow4413$ and $4612\rightarrow2888$ transitions were not strong enough to be verified in the γ-γ coincidence data, the evidence (excitation functions and energies) for their placement is strong. Both have angular distribution and polarizations which establish them definitely as at least partially dipole (as per Fig. 10). This also fixes the 4612-keV level as $J=9$.

The 4713-keV level. The A_2, A_4, and P values of the 101-keV $4713\rightarrow4612$ transition are only consistent with a $J\pm1\xrightarrow{E1}J$ transition and thus $J^\pi=8^-$ or 10^- for the 4713-keV level (compare Fig. 10). The linear polarization measurement which determines $E1$ is shown in Fig. 8. The properties (τ, A_2, A_4, and P) of the 300-keV $4713\rightarrow4413$ transition do not allow an $8^-\rightarrow10^+$ $M2/E3$ transition, e.g., the transition strength would be 18.5 W.u. if it were $M2$. Thus, all data are consistent with a 10^-

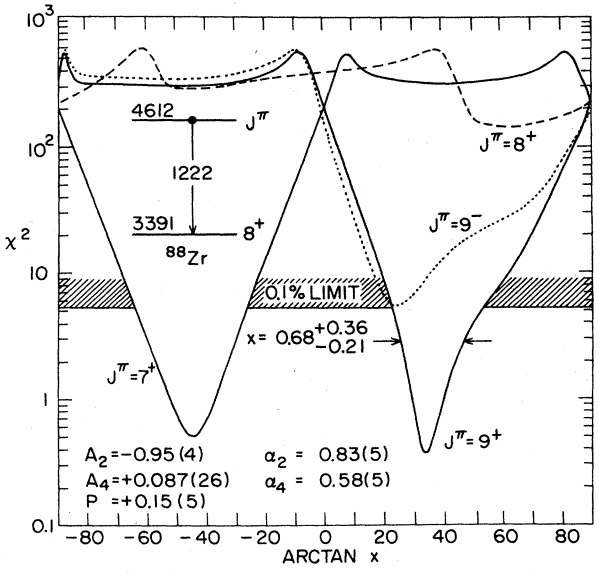

FIG. 15. χ^2 vs arctan$x$ for the ^{88}Zr $4612\rightarrow3391$ transition. The curves are derived from the indicated parameters. The χ^2 values for pure $E2$ $10^+\rightarrow8^+$ and $6^+\rightarrow8^+$ transitions are 400 and 380, respectively. For $J^\pi=7^-$ and 8^-, the curves are everywhere above 7.1 and 110, respectively.

assignment which we consider definite.

The 4798-keV level. The 85-keV 4798→4713 transition is definitely $J\pm1\rightarrow J$ and essentially pure $M1$. Hence $J^\pi=9^-$ or 11^- for the 4798-keV level. The properties of the 385-keV decay to the 10^+ 4413-keV level strongly favor 11^-. For 9^- the measured A_2 and P values are too large in magnitude and yield a minimum $\chi^2=4.3$ (i.e., just below the 0.1% confidence level); for 11^-, $\chi^2_{\min}=0.6$. The reaction mechanism and the absence of crossover transitions to lower-lying $J=7$, 8, and 9 levels also support a $J^\pi=11^-$ assignment. We consider that a 11^- assignment can be made to the 4798-keV level.

The 4486- and 3484-keV levels. Taken together, the properties of the two transitions in the $4713(10^-)\rightarrow4486(J^\pi)\rightarrow3391(8^+)$ cascade demand $J^\pi=9^-$. The properties of the 1003-keV 4486→3484 transition favor $9\xrightarrow{E2}9\pm2$ or $9\rightarrow9$; while the decay modes of the 3484-keV level strongly disfavor $J>7$. Thus $J=7$ is preferred for the 3484-keV level. The 945-keV 3484→2539 transition was obscured by a ^{88}Y 3257→2312 transition. However, in both previous investigations[13,14] this transition was observed to have a characteristic $J+2\rightarrow J$ angular distribution. This, coupled with our observation of a large positive value of P for the composite 945-keV peak, strongly suggests 7^- for the 3484-keV level. Thus, the cumulative evidence rules sufficiently in favor of odd parity for the two levels so that definite 7^- and 9^- assignments can be made to the 3484- and 4486-keV levels, respectively.

The 5166-keV level. The placement of the 369-keV γ ray as 5166→4798 is not certain and thus neither is the existence of the 5166-keV level. If it indeed exists it has $J=10$, 11, or 12 with the latter preferred (R1).

The 5229-keV level. The 816-keV 5229→4413 transition is characteristic of a stretched $12^+\rightarrow10^+$ $E2$ transition ($\chi^2=0.5$) with χ^2 vs arctan$x$ curves for the other possibilities essentially the same as Fig. 9 and as the 4413→3391 transition. The 5229-keV level is given a definite $J^\pi=12^+$ assignment.

The 5666- and 5951-keV levels. From the χ^2 vs arctan$x$ curves and the lifetime restrictions on quadrupole admixtures (Table IV), the 285-keV 5951→5666 and 721-keV 5951→5229 transitions are both definitely $J\pm1\rightarrow J;M1$. The 436-keV 5666→5229 transition is at least partially dipole [$x(E2/M1)<0.16$]. Therefore the 5666-keV level has $J^\pi=12^+$ and the 5951-keV level is 11^+ or 13^+. The reaction mechanism favors $J=13$ but we regard this assignment as not quite definite.

The 6239- and 6501-keV levels. Both the 288-keV 6239→5951 and 551-keV 6501→5951 transitions are $J+1\rightarrow J;M1$, with $J-1\rightarrow J$ excluded at the 0.1% confidence limit so that an assignment of $J^\pi=(14)^+$ is given to both levels. The uncertainty in the assignment, denoted by the parentheses, is due to that in the 5951-keV level.

The 6827-keV level. The 325-keV 6827→6578 transition is definitely $J\pm1\rightarrow J;M1$ and with this restriction the 588-keV 6827→6239 transition is also $J\pm1\rightarrow J;M1$. Invoking the reaction mechanism, $J^\pi=(15)^+$ for the 6827-keV level.

The 5584- to 11200-keV levels. Analysis for the levels on the left-hand side in Fig. 3 with $E_x>5.5$ MeV is straightforward and is adequately summarized in Table IV and Fig. 3.

B. ^{90}Zr

1. Lifetime measurements

DSAM. For the 11404→10765→10126 cascade we measure only the average $F(\tau)$ for the unresolved 639-keV doublet. However, since the 10765-keV level is fed 86(30)% via deexcitation of the 11404-keV level, constraints on the individual $F(\tau)$ lead to the lifetimes given in Table III, where the rather large quoted errors reflect the uncertainty in this unfolding. Similarly, the relative uncertainties in feedings propagate down the decay chain giving rise to successively larger fractional errors in the quoted lifetimes. With the exception of the 1168-keV 10126→8958 transition, all transitions for which a nonzero Doppler shift was observed are too fast to be pure quadrupole, so that $\Delta J\leq1$. Finally, all transitions from levels below $E_x=8$ MeV showed no discernible Doppler shift in the DSAM data.

RDM. The recoil distance data were sufficient to determine (or set limits on) the lifetime of seven of the levels between 5 and 8 MeV. Pertinent data are shown in Fig. 16. The cascade population of the 7438-keV level corresponds to an effective feeding lifetime of $\tau_1=1.62$ ps, as determined from the observed $F(\tau_1)$ for the 621-keV transition. As shown in Fig. 16 and Table III, the RDM data for the 7438- and 7224-keV levels are well fitted for lifetimes $\tau=4.2(7)$ and 85(15) ps, respectively. In these cases the 214-, 270-, and 215-keV γ rays were observed with the planar Ge detector at $\theta_\gamma=0°$.

The subsequent deexcitation γ rays from the levels at 7194, 6954, 6376, 5792, and 5644 keV all exhibit a characteristic decay of ~85 ps, indicating the RDM data on the γ-ray deexcitations is dominated by the feeding lifetime of the 7224-keV level.

For these latter states, two qualitative observations are further evident: (i) there may be a long-lived component ($\tau\gg85$ ps) comprising some ~10% of the total γ-ray intensity, and (ii) there is no evidence for a fast direct-feeding ($\tau\lesssim10$ ps), as might be observed for $D<50$ μm. These observations could be at least partially explained under the assumption that there is a weak (~10%) feeding involving an unobserved "isomeric" transition, coupled with the reasonable expectation that there may be some weak undetected cascade transitions.

In view of these uncertainties, we choose to interpret the latter RDM data on the deexcitation of these states as representing upper limits on the lifetimes involved, as given in Table III.

2. Synthesis of results

As in the case of ^{88}Zr, the properties of the 3589-keV 8^+ isomer and the levels below it are taken from previous investigations.[10,12] And, as for ^{88}Zr, the data summarized are consistent with previous spin-parity assignments and in some cases are an independent determination of them. The results of a simultaneous analysis of the angular distribution, linear polarization, and lifetime data of Table

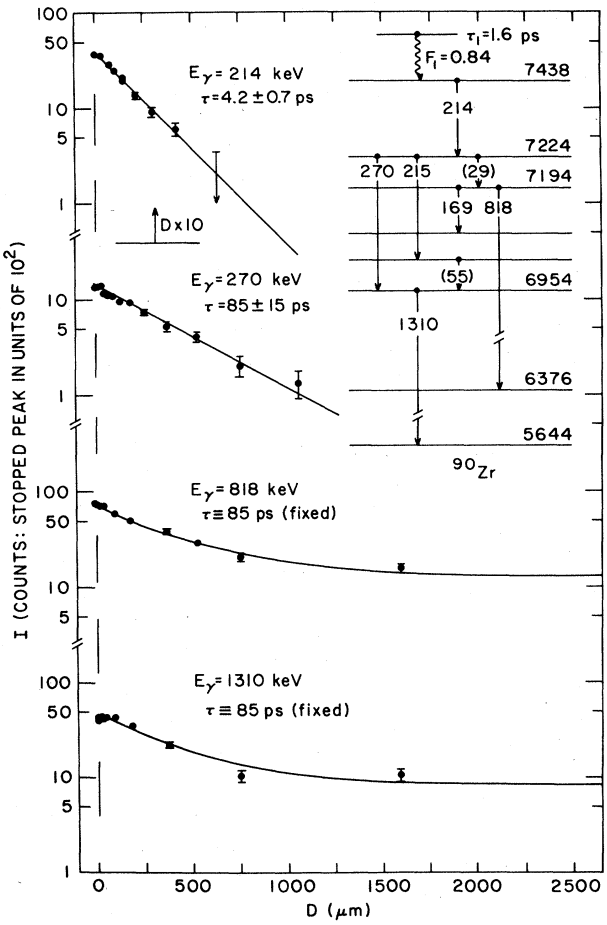

FIG. 16. RDM data for transitions in ^{90}Zr. The ordering of the cascades in the level scheme is shown in the inset: parentheses enclose transitions for which no RDM data were obtained. For the 214- and 270-keV transitions this feeding has been explicitly accounted for (see data, Table III), resulting in the solutions for τ indicated. The data on the 818- and 1310-keV transitions are well fitted for a single lifetime fixed at 85 ps, indicating the measured decay of these lower-lying states is determined almost wholly by the 85-ps lifetime of the 7224-keV level deexcitation.

III are collected in Table V. The following discussion of the individual ^{90}Zr levels above the 8^+ isomer relies heavily on this table.

The 5164-keV level. This level is populated in ^{90}Nb(β^+/EC) and was fixed as $J^\pi=7^-$, 7^+, or 8^+ by Pettersson *et al.*[37] The decay to it from the $J^\pi=10^+$ 7026-keV level (see the following) selects the 8^+ alternative since an $E3$ or $M3$ transition would not be expected to compete with the other observed dipole decay modes from the 7026-keV level.

The 5247-keV level. This level is also populated by the decay of the $J^\pi=8^+$ ^{90}Nb ground state and, from its logft, the decay is allowed or first-forbidden, $J^\pi=6^-$, $7^\pm$, $8^\pm$, $9^\pm$, or 10^-. Of these, 6^- and 10^- can be eliminated since the 1658-keV 5247→3589 transition is too fast to be $M2$ (RUL). Fits to the angular distribution and linear polarization data for this intense transition assuming $J^\pi=7^+$, 8^+, or 9^+ are shown in Fig. 17. Since P is small (consistent with zero), the fits for $J^\pi=7^-$, 8^-, and 9^- are similar. $J=9$ is demanded by these data, and, invoking the RUL, the large $M2/E1$ mixing ratio for $J^\pi=9^-$ rules out that possibility; hence, $J^\pi=9^+$ for the 5247-keV level.

The 5644-keV level. The analysis of the angular distribution and linear polarization data shown in Fig. 9 was discussed in Sec. II F 2. The $J^\pi=6^-$ and 10^- possibilities are ruled out by the lifetime limit (RUL) and also by the data of Fig. 9, i.e., χ^2 is everywhere greater than 120 and 60 for $J^\pi=6^-$ and 10^-, respectively. For $J^\pi=7^-$, 8^-, and 9^-, χ^2 is everywhere greater than 110, 26, and 82, respectively; while for pure $E1$ radiation $\chi^2>800$, 200, and 600, respectively. A $J^\pi=10^+$ assignment is thus definite.

The 5792-keV level. The angular distribution of the 2203-keV 5792→3589 transition rules out pure quadrupole $J\pm2\rightarrow J$ radiation (R6a; $\chi^2=110$) and a $J\rightarrow J$ transition [$\chi^2>16$, for all values of $x(M2/E1)$ or $x(E2/M1)$]. $J^\pi=7^\pm$ and $9^\pm$ give acceptable fits, but for odd parity an appreciable $M2$ component is indicated, i.e., $\chi^2=5.3$ and 12.0 for pure $E1$ radiation and $J^\pi=9^-$ and 7^-, respectively. In any case, $J^\pi=7^\pm$ are strongly ruled against by the decay to the 5792-keV level from the $J=(10)$ level at 7026 keV (see the following). We assume $J^\pi=9^{(+)}$.

The 6280-keV level. The data from the 1032-keV 6280→5247 transition give a classic $J+2\rightarrow J$ $E2$ χ^2 vs arctan$x$ plot similar to Fig. 9 with $\chi^2=0.84$ for pure $E2$ radiation. The $J\pm1\rightarrow J$ alternatives are ruled against with $\chi^2>20$ for all mixing ratios. However, an

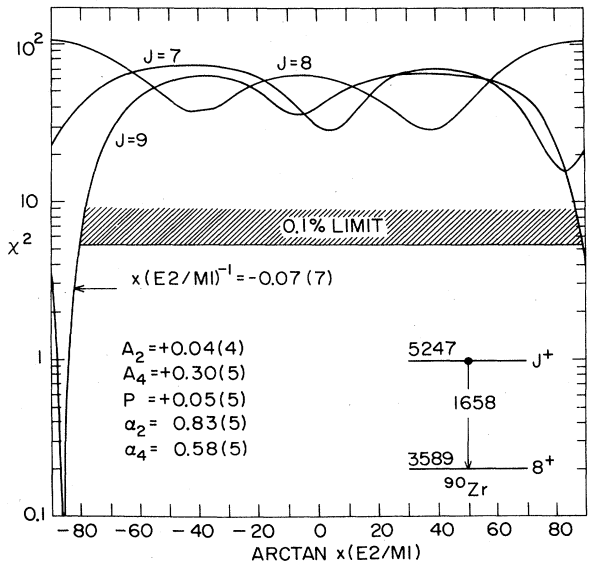

FIG. 17. χ^2 vs arctan$x$ for the ^{90}Zr 5247→3589 transition. The curves are based on the listed parameters. Since P is small and consistent with zero, the curves for $\pi=-$ are similar.

TABLE V. ^{90}Zr branching ratios, partial lifetimes, mixing ratios, and transition strengths.

E_i (keV)	E_f (keV)	E_γ (keV)	Branching ratio[a] (%)	τ(partial)[b] (ps)	Dominant multipole	$x(L+1/L)$[c]	$B(L)$[d] (W.u.)	$B(L+1)$[d] (W.u.)	Conclusions and remarks
5164	3589	1575	43(6)		$M1$				J^π from β^+ and 7026→5164
	3448	1716	57(6)		[$E2$]				None
5247	3589	1658	100	<40	$E2$[e]	$[-0.07(7)]^{-1}$		>0.05	$J+1\rightarrow J;M1$ (see Fig. 17 and the text)
5644	3589	2055	100	<40	$E2$	(0)	>0.02		$J+2\rightarrow J;E2$ (see Fig. 9 and the text)
5792	3589	2203	100		($M1$)	$+0.07(4)$[e]			$J+1\rightarrow J;(M1)$[f]
6280	5247	1032	100		($E2$)	(0)			$J+2\rightarrow J;(E2)$ preferred[f]
6376	5792	584	22(12/6)		($M1$)				($M1$) from P
	5247	1128	78(8)		[$M1$]				Doublet
6721	6376	345	69(3)		[$M1$]				$(J\rightarrow J)$[i]
	5247	1474	31(3)		[$M1$]				None
6770	6280	490	100		($M1$)	$+0.26(6)$[e]			$J\pm1\rightarrow J;(M1)$[f]
6954	5644	1310	100	<40	$E1$	<0.26[g]; $-0.02(2)$[e]	$>5.4\times10^{-6}$		$J\pm1\rightarrow J;E1$[f],$(J+1\rightarrow J)$[j]
7009	6954	55	13(2)		[$E1$]				$(J\rightarrow J)$[i]
	6721	288	50(2)		$M1$	$+0.07(5)$[e]			$J\pm1\rightarrow J;M1$
	5644	1365	37(2)		($E1$)	$+0.01(2)$[e]			$J\pm1\rightarrow J;(E1)$
7026	5792	1234	17(3)		[$M1$]				$(J\pm1\rightarrow J)$[i]
	5644	1382	6(1)		[$M1$]				None
	5247	1778	61(3)		[$M1$]				Triplet
	5164	1861	16(2)		($E2$)				$(J\pm2\rightarrow J;E2)$
7194	7026	169	30(1)	<140	$M1$	<0.24[g]	>0.05		$J\pm1\rightarrow J;M1$[f,g]
	6376	818	67(1)	<60	$E1$	<0.10[g]; $+0.02(4)$[e]	$>1.4\times10^{-5}$		$J\pm1\rightarrow J;E1$[f,g]
	5644	1550	3(1)	$<2\times10^3$	[$M1$]		$>4.3\times10^{-6}$		$(J\pm1\rightarrow J)$[i]
7224	7194	30	47(2)	$1.4(3)\times10^3$	$M1$	<0.008[g]	0.87(13)		$J\pm1\rightarrow J;M1$[k,g]
	7009	215	17(1)	500(90)	[$M1$]	<0.82[g]	$6.4(10)\times10^{-3}$		$(J\pm1\rightarrow J)$[i,g]
	6954	270	35(2)	243(44)	$E1$	<0.013[g]; $+0.02(3)$[e]	$1.02(14)\times10^{-4}$		$J\pm1\rightarrow J;E1$[f,g]
	5644	1580	0.9(2)	$9.4(26)\times10^3$	($E2$)		$3.7(10)\times10^{-4}$		$(J\pm2\rightarrow J;E2)$
7438	7224	214	100	4.2(7)	$M1$	<0.08[g]; $+0.07(3)$[e]	0.77(11)	<340	$J\pm1\rightarrow J;M1$[f,g]
8058	7438	621	100	0.4(2)	$M1$	<0.5[g]; $+0.14(5)$[e]	0.33(17)	18(13)	$J\pm1\rightarrow J;M1$[f,g]
8958	8058	900	100	0.7(4)	$E1$	<0.02[g]; $+0.07(7)$[e]	$9.5(54)\times10^{-4}$		$J\pm1\rightarrow J;E1$[f,g]
(9707)	8958	749	100	≤0.7(2)	($M1$)	<0.76[g]; $+0.15(15)$[e]	>0.11(3)	≥5(14/5)	$J\pm1\rightarrow J;(M1)$[f,g]
9836	8058	1778	100		[$M1$]				Unresolved triplet
10126	9836	290	36(2)	2.5(8)	$M1$	<0.16[g]; $+0.01(6)$[e]	0.52(17)		$J\pm1\rightarrow J;M1$[f,g]
	8958	1168	64(2)	1.4(5)	$E1$	<0.05[g]; $+0.02(5)$[e]	$2.2(8)\times10^{-4}$		$J\pm1\rightarrow J;E1$[f,g]

TABLE V. (*Continued*).

E_i (keV)	E_f (keV)	E_γ (keV)	Branching ratio[a] (%)	τ(partial)[b] (ps)	Dominant multipole	$x(L+1/L)$[c]	$B(L)$[d] (W.u.)	$B(L+1)$[d] (W.u.)	Conclusions and remarks
10765	10126	639	100	<0.6	($M1$)	<0.5[g]	>0.20		($J\pm1\rightarrow J;M1$)[f,g]
11404	10765	639	100	0.3(2)	($M1$)	<0.5[g]	0.4(3)		($J\pm1\rightarrow J;M1$)[f,g]
12111	11404	707	100	0.20(7)	($M1$)	<0.4; +0.3(5)[e]	0.45(16)		($J\pm1\rightarrow J;M1$)[f,g]
12965	12111	854	100	<0.5	[$M1$]	<0.8[g]			Dipole[g]

[a]The γ branching in percent.
[b]From the branching ratio and the level lifetime of Table III. The lifetime is for the γ transition only, i.e., a correction has been made for internal conversion when significant.
[c]The $E2/M1$ or $M2/E1$ mixing ratios (amplitudes) from analysis of the angular distribution and linear polarization measurements together with any restrictions imposed by the measured partial lifetimes and the RUL (see the text). Values in brackets are assumed. The sign convention is that of Ref. 34.
[d]The transition strengths (in W.u.) of the lowest allowed multipole (L) and next-lowest allowed multipole ($L+1$) from τ(partial) and $x(L+1/L)$.
[e]Note that the reciprocal of $x(L+1/L)$ for $J+1\rightarrow J$ is given, i.e., the transition is predominantly $E2$.
[f]From A_2, A_4, and P.
[g]From the partial lifetime and the RUL's. The limit is for the absolute magnitude.
[h]For $J\pm2\rightarrow J$.
[i]From the angular distribution.
[j]Preferred by the reaction mechanism.
[k]From the internal conversion coefficient—see the text.

$M1/E2$ $J\rightarrow J$ transition and an $E2$ $J-2\rightarrow J$ transition are not completely ruled out, $\chi^2>3.2$ and $\chi^2=4.0$ for these two cases, respectively. Thus $J+2\rightarrow J$ is preferred by the γ-decay data and by the reaction mechanism (R5) but is not considered definite. The parity is fixed as even since a $M2/E1$ mixture for $J\rightarrow J$ is ruled out ($\chi^2>8.0$). Thus $J^\pi=(11)^+$.

The 6770-keV level. For the 6770→6280 transition $J\pm2\rightarrow J$ can be excluded (R6a) as can $J\rightarrow J$ ($\chi^2>42$). Either of $J\pm1\rightarrow J$ is allowed with very similar mixing ratios for the $E2/M1$ and $M2/E1$ alternatives. Since sizable $M2$ radiation would be demanded, the $E2/M1$ mixture is favored. Of these, $J+1\rightarrow J$ is favored by the reaction mechanism. Thus, $J^\pi=(12^+)$.

Assignments for the remainder of the levels can be inferred from the data of Tables III and V using similar arguments to those presented so far for ^{88,90}Zr. The ^{90}Zr assignments are not as clear-cut as for ^{88}Zr because (1) there are several unfortunate energy degeneracies (or near degeneracies) such as the 1128-keV 6376→5247 and 3448→2319 transitions and the 214-keV 7438→7224 and 7224→7009 transitions; (2) the RDM lifetime information was meager because of the dominance of the 85-ps lifetime for the 7224-keV level; and (3) most of the transitions observed above the 8^+ isomer are $J\pm1\rightarrow J$ and these two alternatives are the most difficult to tell apart. Because of such difficulties, all spin assignments to levels above that at 5644 keV rely on the reaction mechanism favoring of $J+1\rightarrow J$ over $J-1\rightarrow J$ transitions and therefore are considered as somewhat uncertain. However, in many cases where the spin is uncertain the parity is not.

The 30-keV 7224→7194 transition is a special and important case for which a few words are necessary. Because of its low energy this transition was initially overlooked in the γ-γ coincidence, angular distribution, and excitation function measurements. Its presence was inferred from the γ-γ data, e.g., the 214- and 818-keV transitions were strongly in coincidence. Thus, a special series of measurements were carried out to determine the properties of this transition. An unexpected complication in these measurements was encountered when it was found that the sought for 30-keV γ transition was actually a doublet, the other member being a 2151→2121 transition in ^{89}Zr. The properties of these two transitions were untangled using the ^{74}Ge and ^{76}Ge excitation functions and angular distributions.

Based upon the lifetime of the 7224-keV level, the 30-keV transition must be dipole: even as such it is highly converted with an internal conversion coefficient $\alpha=3.67$ and 6.81 for $E1$ and $M1$, respectively. The large difference between these two alternatives allows a determination of the multipolarity from intensity measurements. From a comparison of the relative intensities of the 818- and 1310-keV transitions in coincidence with γ rays from the decay of levels above the 7224-keV level (see Fig. 4), it is an easy matter to obtain the total transition intensity (T_T) for the 30-keV transition. Comparison to I_γ (from singles measurements) yields $\alpha=6.2(10)$ in agreement with $M1$ radiation but not $E1$ radiation. The angular distribution excludes a $J\rightarrow J$ transition for this essentially pure dipole transition and we assume $J+1\rightarrow J$ because of the reaction

mechanism (R5).

There are five additional γ rays listed in Table III which seem to belong to ^{90}Zr but for which there is not enough evidence to place them in the decay scheme. From the γ-γ information, the 731-keV transition appears to feed directly into the 5644-keV level, and as such it should depopulate a level at 6375.09(20) keV. This could conceivably be the same level as the 6376.06(8)-keV level (Table III and Fig. 4), but (1) the energy agreement is poor and (2) the evidence from A_2, A_4, and P strongly suggests $J\pm1\rightarrow J;M1$ [with $x(E2/M1)=-0.21(5)$ for a $J+1\rightarrow J$ assignment to the 731-keV transition], rather than $J\rightarrow J;E1$ as expected for this placement.

IV. SHELL-MODEL DESCRIPTION OF ^{88,90}ZR

^{90}Zr is well known to be a quasimagic nucleus, lying on the $N=50$ neutron shell closure and at $Z=40$ which, in spherical nuclei, represents the filling of the fp shell with the $1g_{9/2}$ shell empty above. Because the $N=50$ shell gap and the gap between the $f_{7/2}$ and $f_{5/2}$, $p_{3/2}$, and $p_{1/2}$ subshells are considerably larger than the $Z=40$ subshell closure, the low-lying even parity states can be presumed to arise largely from $\pi[(f_{5/2},p_{3/2},p_{1/2})^{-2}g_{9/2}^2]$ configurations. The maximum angular momentum that can be generated from this 2p-2h excitation is $J_{\max}=12$, and in order to gain more angular momentum either four-particle proton excitations such as

$$\pi[(f_{5/2}p)^{-n}(g_{9/2})^n;n=2,4] \tag{16a}$$

are required, or we must invoke the breaking of the neutron shell closure to form states of the type

$$\{\pi[(f_{5/2}p)^{-m}(g_{9/2})^m;m=0,2]$$
$$\times\nu[(g_{9/2})^{-n}(d_{5/2})^n;n=1,2]\}\ . \tag{16b}$$

The first of these has $J^\pi_{\max}=18^+$ and the second has $J^\pi_{\max}=19^+$ $(m,n=2,1)$ and 24^+ $(m,n=2,2)$. Odd-parity states in ^{90}Zr from np-nh states with $n\leq3$ can be generated by

$$\pi[(f_{5/2}p)^{-n}(g_{9/2})^n;n=1,3] \tag{17a}$$

and/or

$$\{\pi[(f_{5/2}p)^{-1}(g_{9/2})]\nu[(g_{9/2})^{-n}(d_{5/2})^n];n=1,2\} \tag{17b}$$

with $J^\pi_{\max}=7^-$ $(n=1)$ and 16^- $(n=3)$ for the first of these [Eq. (17a)] and $J^\pi_{\max}=14^-$ $(n=1)$ and 19^- $(n=2)$ for the second [Eq. (17b)]. Previous shell-model calculations for ^{90}Zr as reviewed by Chiang, Wang, and Han[38] have been confined to the closed $g_{9/2}$ neutron orbit and, at most, two proton excitations from the $(f_{5/2},p)$ shell to the $g_{9/2}$ shell, i.e.,

$$\pi[(f_{5/2}p)^{-n}(g_{9/2})^n;n=1,2]\ .$$

Because of the unfilled $g_{9/2}$ neutron shell the yrast spectrum of ^{88}Zr reaches higher spin more simply than that of ^{90}Zr. The model space used for ^{88}Zr is

$$\{\pi\nu[(f_{5/2}p)^{-n}(g_{9/2})^{8+n};n=0,1,2,3]\}\ , \tag{18}$$

where the even-parity states correspond to $n=0+2$ and the odd-parity states to $n=1+3$. Only states with $J\geq12$ were calculated with $n=3$. The space of Eq. (18) generates states up to $J^\pi_{\max}=20^+$ and 24^-. The largest basis used in previous[39] shell-model calculations of ^{88}Zr was

$$\{\pi[(p_{1/2})^{-n}(g_{9/2})^n]\nu[(g_{9/2})^{-2}]\}$$

with $n=1$ and 2 for odd parity and even parity, respectively.

Thus, in order to attempt an understanding of the level schemes of ^{88,90}Zr, a large-basis shell-model calculation was undertaken with the Livermore m-scheme computer code.[40] The nucleon-nucleon interaction used was that of Petrovich *et al.*[41] which is a realistic state-independent interaction based on the Kallio-Kolltveit interaction. $M1$ and $E2$ transition rates and moments were calculated as well as energy level spectra. At the present time only preliminary results of these calculations are available; the full results will be published separately.[42]

In the m scheme, limitations on the complexity of the configurational space decreases as the minimum J included in the calculations increases. Thus for the even-parity states of ^{90}Zr, only $\pi[(f_{5/2}p)^{-2}(g_{9/2})^2]$ could be included for $J^\pi<8^+$. For $J^\pi\geq8^+$ the full 2p-2h and 4p-4h proton space of Eq. (16a) could be used, and for $J\geq12$ a calculation was also made in the neutron-proton space of Eq. (16b). The principal of J matching was used to tie the latter two calculations to the first. That is, in both calculations in the basis of Eq. (16), it is found that the lowest-lying states considered are predominantly $\pi[(f_{5/2}p)^{-2}(g_{9/2})^2]$, thus the spectrum for the more complicated calculations are shifted in energy to match the states from the simplest calculation which overlap with them. For the odd-parity levels, both 1p-1h and 3p-3h proton excitations [Eq. (17a)] were considered for all possible J. Examples of these calculations are given in Figs. 18 and 19 where comparison is made to experiment for ^{90}Zr.

Considering that the nucleon-nucleon interaction used is a realistic one, i.e., not specifically tuned to the mass 90 region, the calculations give a quite reasonable description of the experimental results. In particular, both ^{88}Zr and ^{90}Zr energy level spectra were reproduced quite well. For ^{90}Zr, however, the spectrum could be reproduced fairly well for $J\geq12$ using the basis of *both* Eqs. (16a) and (16b) indicating that the even-parity states of ^{90}Zr with $J\geq12$ (and perhaps $J<12$) contain large admixtures of both proton and neutron excitations. A crucial test of the calculation is provided by the experimentally large $M1$ transition strengths in the sequence $14^+\rightarrow13^+\rightarrow12^+\rightarrow11^+$ starting at the 8058-keV level of ^{90}Zr (see Table V). The states generated from proton excitations alone do not give agreement with these observed rates—in general they are considerably too weak. For the states generated from neutron excitations, i.e., the basis of Eq. (16b), the $14^+_1\rightarrow13^+_1\rightarrow12^+_1$ sequence has $M1$ rates of 1.70 and 1.85 W.u., respectively, while the $13^+_1\rightarrow12^+_2$ $M1$ transition strength is ~0 W.u. Unfortunately, at the present time the $12^+\rightarrow11^+$ part of the cascade has not been calculated

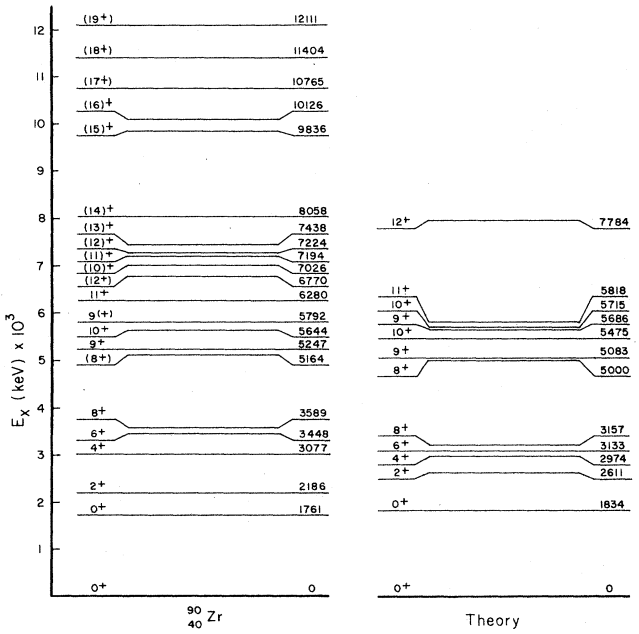

FIG. 18. Even-parity experimental and calculated ^{90}Zr level scheme. The model space for the calculation is that of Eq. (16a). Only the one or two lowest lying states of a given J are included in the theoretical spectrum.

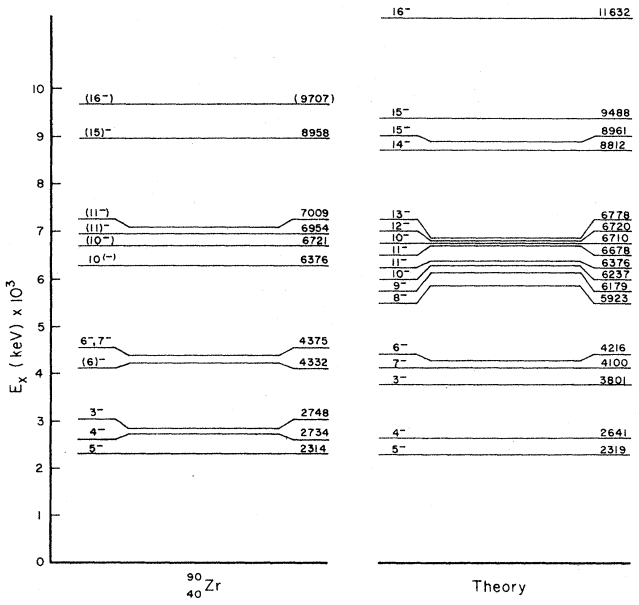

FIG. 19. Odd-parity experimental and calculated ^{90}Zr level scheme. The model space for the calculation is that of Eq. (17a). Only the one or two lowest lying states of a given J are included in the theoretical spectrum.

because of difficulties in fitting states with $J \leq 11$ into the computer for the basis of Eq. (16b). However, the model space in question does seem capable of generating the large $M1$ strengths seen experimentally.

For ^{88}Zr, the calculations give a good account of the observed spectra and of many of the observed transition rates. For instance, the energy spacing between the lowest two 8^+ states is predicted about right and the high selection of the lowest 9^+ and 10^+ states for decay to 8_2^+ rather than 8_1^+ is reproduced.

In conclusion, then, it appears that the observed yrast spectra of ^{88,90}Zr can be interpreted as arising from intrinsic modes of excitation with no evidence for collective behavior at even the highest observed angular momenta.

ACKNOWLEDGMENTS

The Ge target preparation was performed by Irving Feigenbaum whom we thank for his careful and successful fabrication of these difficult targets. Thanks are due to S. D. Bloom for his advice and his participation in the shell model calculations outlined in Sec. IV. Research supported at Brookhaven National Laboratory under the auspices of the U.S. Department of Energy, Division of basic Energy Sciences, under Contract No. DE-AC02-76CH00016 and at Lawrence Livermore Laboratory under Contract No. W-7405-ENG-48. One of us (C.J.L.) was also partially supported by a grant from the Science and Engineering Research Council (UK).

*Present address: University of Manchester, Manchester, England.

†Permanent address: University of Pennsylvania, Philadelphia, PA 19104.

[1]C. J. Lister, B. J. Varley, H. G. Price, and J. W. Olness, Phys. Rev. Lett. **49**, 308 (1983); H. G. Price, C. J. Lister, B. J. Varley, W. Gelletly, and J. W. Olness, *ibid.* **51**, 1842 (1983); (unpublished).

[2]S. Åberg, Phys. Scr. **25**, 23 (1982).

[3]P. Möller and J. R. Nix, At. Data Nucl. Data Tables **26**, 165 (1981).

[4]I. Ragnarsson, S. G. Nilsson, and R. K. Sheline, Phys. Rep. **45**, 1 (1978).

[5]D. Bucurescu *et al.*, Rev. Roum. Phys. **24**, 971 (1979).

[6]S. Åberg, R. Bengtsson, I. Ragnarsson, and J. Zhang, in *Proceedings of the Nuclear Physics Workshop, International Center for Theoretical Physics, Trieste, Italy, 1981,* edited by C. H. Dasso (North-Holland, Amsterdam, 1982).

[7]J. H. Hamilton *et al.*, in *Proceedings of the Fourth International Conference on Nuclei far from Stability, Helsingør, Denmark, 1981,* edited by P. G. Hansen and G. B. Nielsen (CERN, Geneva, 1981); H. P. Hellmeister *et al.*, Phys. Lett. **85B**, 34 (1979).

[8]C. J. Lister, B. J. Varley, D. E. Alburger, P. E. Haustein, S. K. Saha, J. W. Olness, H. G. Price, and A. D. Irving, Phys. Rev. C **28**, 2127 (1983); J. Panqueva, H. P. Hellmeister, F. J.

Bergmeister, and K. P. Lieb, Phys. Lett. **98B**, 248 (1981).
[9]R. L. Bunting and J. J. Kraushaar, Nucl. Data. **18**, 87 (1976).
[10]D. C. Kocher, Nucl. Data **16**, 55 (1975).
[11]K. Oxorn and S. K. Mark, Z. Phys. A **316**, 97 (1984).
[12]E. K. Warburton and D. E. Alburger, Phys. Rev. C **26**, 2595 (1982).
[13]J. E. Kitching, P. A. Batay-Csorba, C. A. Fields, R. A. Ristinen, and B. L. Smith, Nucl. Phys. **A302**, 159 (1978).
[14]T. Numao, H. Nakayama, T. Kobayashi, T. Shibata, and Y. Kuno, J. Phys. Soc. Jpn. **46**, 361 (1979).
[15]J. T. Routti and S. G. Prussin, Nucl. Instrum. Methods **72**, 125 (1969).
[16]R. G. Helmer, P. H. M. van Assche, and C. van der Leun, At. Data Nucl. Data Tables **24**, 39 (1979).
[17]R. C. Lee and R. A. Scheetz, IEEE Trans. Nucl. Sci. **NS-26**, 4405 (1979).
[18]A. M. Nathan, J. W. Olness, E. K. Warburton, and J. B. McGory, Phys. Rev. C **16**, 192 (1977).
[19]F. Puhlhofer, Nucl. Phys. **A280**, 267 (1977).
[20]D. C. Kocher, Nucl. Data **16**, 445 (1975).
[21]O. C. Kistner, A. W. Sunyar, and E. der Mateosian, Phys. Rev. C **17**, 1417 (1978).
[22]This geometry was actually used in the analysis; however, the deviation of the results from those for detection at 90° is practically negligible and for simplicity 90° is assumed in the following discussion.
[23]A. R. Poletti, E. K. Warburton, and J. W. Olness, Phys. Rev. **164**, 1479 (1967).
[24]P. A. Butler, P. E. Carr, L. L. Gadeken, A. N. James, P. J. Nolan, J. F. Sharpey-Schafer, P. J. Twin, and D. A. Viggars, Nucl. Instrum. Methods **108**, 497 (1973).
[25]D. B. Fossan and E. K. Warburton, in *Nuclear Spectroscopy and Reactions,* edited by J. Cerny (Academic, New York, 1974), Part C, p. 307.
[26]A. E. Blaugrund, Nucl. Phys. **88**, 501 (1966).
[27]T. Yamazaki, At. Data Nucl. Data Tables **3**, 1 (1967).
[28]R. M. Diamond, E. Matthias, J. O. Newton, and F. S. Stephens, Phys. Rev. Lett. **16**, 1205 (1966).
[29]G. A. P. Engelbertink, L. P. Eckström, D. E. C. Scherpenzeel, and H. H. Eggenhuisen, Nucl. Instrum. Methods **143**, 161 (1977).
[30]L. O. Eckström, A. M. Al-Naser, P. R. G. Lornie, and P. J. Twin, Nucl. Instrum. Methods **158**, 243 (1979).
[31]P. M. Endt, At. Data Nucl. Data Tables **23**, 547 (1979).
[32]S. J. Skorka, J. Hertel, and T. W. Retz-Schmidt, Nucl. Data **2**, 347 (1966).
[33]P. Taras and B. Haas, Nucl. Instrum. Methods **123**, 73 (1975).
[34]For mixing ratios we use the sign convention of H. J. Rose and D. M. Brink, Rev. Mod. Phys. **39**, 306 (1967).
[35]D. Pelte and D. Schwalm, in *Heavy Ion Collisions,* edited by R. Bock (North-Holland, Amsterdam, 1982), Vol. 3.
[36]S. Raman and N. B. Gove, Phys. Rev. C **7**, 1995 (1973).
[37]H. Pettersson, S. Antman, and Y. Grunditz, Nucl. Phys. **A108**, 124 (1968).
[38]H. C. Chiang, M. C. Wang, and C. S. Han, J. Phys. G **6**, 345 (1980).
[39]D. H. Gloeckner and F. J. D. Serduke, Nucl. Phys. **A220**, 477 (1974).
[40]R. F. Hausman, Jr., University of California Radiation Laboratory Report No. UCRL-52178, 1976.
[41]F. Petrovich, H. McManus, V. A. Madsen, and J. Atkinson, Phys. Rev. Lett. **22**, 895 (1969).
[42]J. A. Becker, S. D. Bloom, and E. K. Warburton (unpublished).